SOME BOUND EXCITON PROCESSES IN CADMIUM SULPHIDE

by

Melvin Douglas Smeaton

B.Sc. (Honors), University of Alberta, 1971

A THESIS SUBMITTED IN PARTIAL FULFILLMENT OF

THE REQUIREMENTS FOR THE DEGREE OF

MASTER OF SCIENCE

in the Department

of

Physics

SIMON FRASER UNIVERSITY

AUGUST 1973

APPROVAL

Name: Melvin Douglas Smeaton

Degree: Master of Science

Title of Thesis: Some Bound Exciton Processes in Cadmium Sulphide

Examining Committee:

Chairman: R. F. Frindt

R. R. Haering
Senior Supervisor

J. C. Irwin

K. E. Rieckhoff

K. Colbow

Date Approved: August 28, 1973

PARTIAL COPYRIGHT LICENSE

I hereby grant to Simon Fraser University the right to lend my thesis or dissertation (the title of which is shown below) to users of the Simon Fraser University Library, and to make partial or single copies only for such users or in response to a request from the library of any other university, or other educational institution, on its own behalf or for one of its users. I further agree that permission for multiple copying of this thesis for scholarly purposes may be granted by me or the Dean of Graduate Studies. It is understood that copying or publication of this thesis for financial gain shall not be allowed without my written permission.

Title of Thesis/Dissertation:

Some Bound Exciton Processes in Cadmium Sulphide

Author: _____

(signature)

Melvin Douglas SMEATON

(name)

August 28, 1973

(date)

ABSTRACT

The I_2 complex in CdS consists of an exciton weakly bound to a neutral donor, and is essentially a three particle system (two electrons and a hole). When the exciton decays by recombination of the hole and a constituent electron, the remaining electron is left in one of the available states of the isolated donor. These states may be bound hydrogenic states of the neutral donor or unbound coulomb states of the donor core. We have shown, by means of the Sudden Approximation, that knowledge of the luminescence resulting from these transitions may be used to provide an expansion of the donor electron wavefunction, in the presence of the exciton complex, in terms of the bound hydrogenic and unbound coulomb wavefunctions. From consideration of the luminescence resulting from projection of the residual donor electron onto the unbound continuum states, we have estimated the spatial extent of this single electron wavefunction.

Our investigations have uncovered a series of sharp luminescent lines in the wavelength region 5050 to 5100 Å, including two transitions originally reported by Reynolds and Litton (1963). Excitation spectra of these long wavelength lines have enabled us to find a close relationship between the different transitions. We believe that they result from

the radiative decay of two distinct bound exciton complexes, which we have labeled I_6 and I_7 in the notation of Reynolds and Litton (1963). Probably these complexes result from excitons bound to deep impurities in CdS. Results of the excitation spectra have also indicated the presence of a resonant exciton transfer mechanism from the I_2 complex to the more strongly bound state represented by the I_6 complex. We have investigated the effects of variations in excitation intensity and sample temperature on the long wavelength lines, and have measured the thermal activation energy for I_{6a}, a transition of the I_6 complex. On the basis of our experimental results we have constructed a tentative energy level diagram for decay of the I_6 bound exciton.

TABLE OF CONTENTS

LIST OF TABLES

LIST OF FIGURES

ACKNOWLEDGEMENTS

I wish to thank Dr. R. R. Haering for supervising my research and for being a constant source of useful suggestions and ideas. Thanks are due also to the Physics Department, not only for partial financial support through teaching assistantships, but also for interesting graduate courses taught by various department members, and for the help I have received in preparing this thesis.

I would like to express appreciation to Dr. J. C. Irwin for allowing me the use of his Andonian dewar and other essential pieces of equipment for an extended period of time. I am also grateful to Roland Egloff for permitting me to use his experimental apparatus on many occasions. Thanks are due to Ian Easson of U.B.C. for useful discussions regarding the Sudden Approximation, and to Joel Mercier for working over-time to complete the diagrams for this thesis. Also, I acknowledge the National Research Council for their financial support in the form of a scholarship. Finally, I thank my wife Marg for her continuing support.

1. Introduction

The electronic structure and optical properties of bound exciton complexes in Cadmium Sulphide have generated considerable interest, and prompted extensive experimental and theoretical investigations for more than a decade. Recently (Nassau, Henry and Shiever 1970), it was shown that discrete luminescent lines resulting from two-electron transitions, where an exciton bound to a neutral donor decays leaving the donor in an excited state, could be used to obtain precise values of the energy separations between the ground state and excited states of donors in CdS, from which the donor binding energies could be estimated. The luminescent lines reported by Nassau, Henry and Shiever (1970) correspond to observing discrete bound states of the neutral donor. More recently (Malm and Haering 1971a), it was shown that radiative two-electron transitions could be extended to the case where the residual donor electron is promoted into the conduction band. From consideration of a luminescent Auger band resulting from such a process, Malm and Haering (1971a) were able to directly estimate the binding energy of the Cl donor in CdS.

The theoretical and experimental results presented in PART I of this thesis demonstrate, by means of the Sudden Approximation, that the two-electron transitions are a mapping of the donor electron wavefunction, in the presence

of the exciton complex, onto the bound hydrogenic states and the unbound coulomb states of the isolated donor. Also, from knowledge of a luminescent Auger band, resulting from two-electron transitions to the continuum of unbound coulomb states, an estimate is made of the spatial extent of the electron wavefunction in the bound exciton complex.

PART II of this thesis is dedicated to the investigation of a series of long wavelength bound exciton lines in CdS. Reynolds and Litton (1963) were the first to report sharp, discrete luminescent lines in the long wavelength region 5050-5100 Å. While these lines had the appearance of bound exciton emission, there was apparently no connection between them and transitions occurring at much higher energies, associated with well known exciton complexes. There also appears to be no connection with the weak pair-spectra lines which were subsequently reported in CdS (Henry, Faulkner and Nassau 1969; Reynolds and Collins 1969). In addition to the two lines originally reported by Reynolds and Litton (1963), our investigations have uncovered several other strong lines. Through the use of excitation spectra and the effects of temperature and intensity variation, the relationship between the various long wavelength lines is now better understood. Most probably these lines result from the radiative decay of excitons bound to two chemically distinct deep impurities, possibly isoelectronic traps, or deep donors or acceptors.

Experimental evidence is presented which suggests that a resonant exciton transfer takes place between the I_2 complex, an exciton bound to a shallow donor, and the deep complex giving rise to the long wavelength lines.

2. A Brief Review of Exciton Luminescence in CdS

2.1 Intrinsic Excitons in CdS

Excitons in CdS are best described in terms of a weak-binding model developed by Wannier (1937). Wannier excitons are formed from holes and electrons in band states perturbed by the coulombic interaction of the electron and hole. This approximation, which allows the use of effective mass theory in treating the exciton states, is reasonable since the electron-hole coulomb interaction is greatly weakened due to dielectric screening, thus resulting in large exciton Bohr radii which, in CdS, are about 30Å. Reviews of formal exciton theory may be found in D. L. Dexter and R. S. Knox (1965), and R. S. Knox (1963). The early experimental and theoretical development of excitons in CdS was due primarily to a series of fundamental papers by D. G. Thomas and J. J. Hopfield: Thomas and Hopfield (1959), Hopfield and Thomas (1960), and Hopfield (1960). In a subsequent paper, Hopfield and Thomas (1961), a thorough account of the magnetic properties of exciton absorption lines was presented.

On the basis of a tight-binding model it is possible to assign p-like symmetry to the valence bands and s-like symmetry to the conduction band in CdS (Hopfield 1959). At $\vec{k}=0$ the six-fold degenerate (including spin) p-bands are split into three doubly-degenerate bands by means of the crystal field and spin-orbit coupling. The amount of splitting has been

determined by consideration of exciton binding energies (Thomas and Hopfield 1959). A schematic of the energy band configuration at $\vec{k}=0$ is shown in Fig. 1. Once it has been determined to which irreducible representation of the $\vec{k}=0$ crystal double group each band state belongs, the selection rules for dipole transitions may be found. These are indicated in Fig. 1. The character table for the above crystal double group may be found in Hopfield (1960).

Free excitons are labelled according to which band the hole originates from. Thus A excitons are formed from an electron in the conduction band and a hole in the A valence band. As might be predicted from the selection rules for band to band transitions, allowed A exciton transitions at $\vec{k}=0$ are most active for $\vec{E}\perp c$, where $\vec{E}$ is the electric vector defining the polarization of the light, and c is the hexagonal axis of the CdS crystal. B and C excitons are active for both polarizations. (The use of band symmetries to characterize excitons is only an approximation since only the symmetry of the exciton state, not the symmetries of the individual electron and hole alone, is a good quantum number.)

Table I lists the wavelength and energy positions of those exciton states which have been observed experimentally as absorption or luminescent transitions. Some of the lines are labelled in the notation used by Hopfield and Thomas (1961),

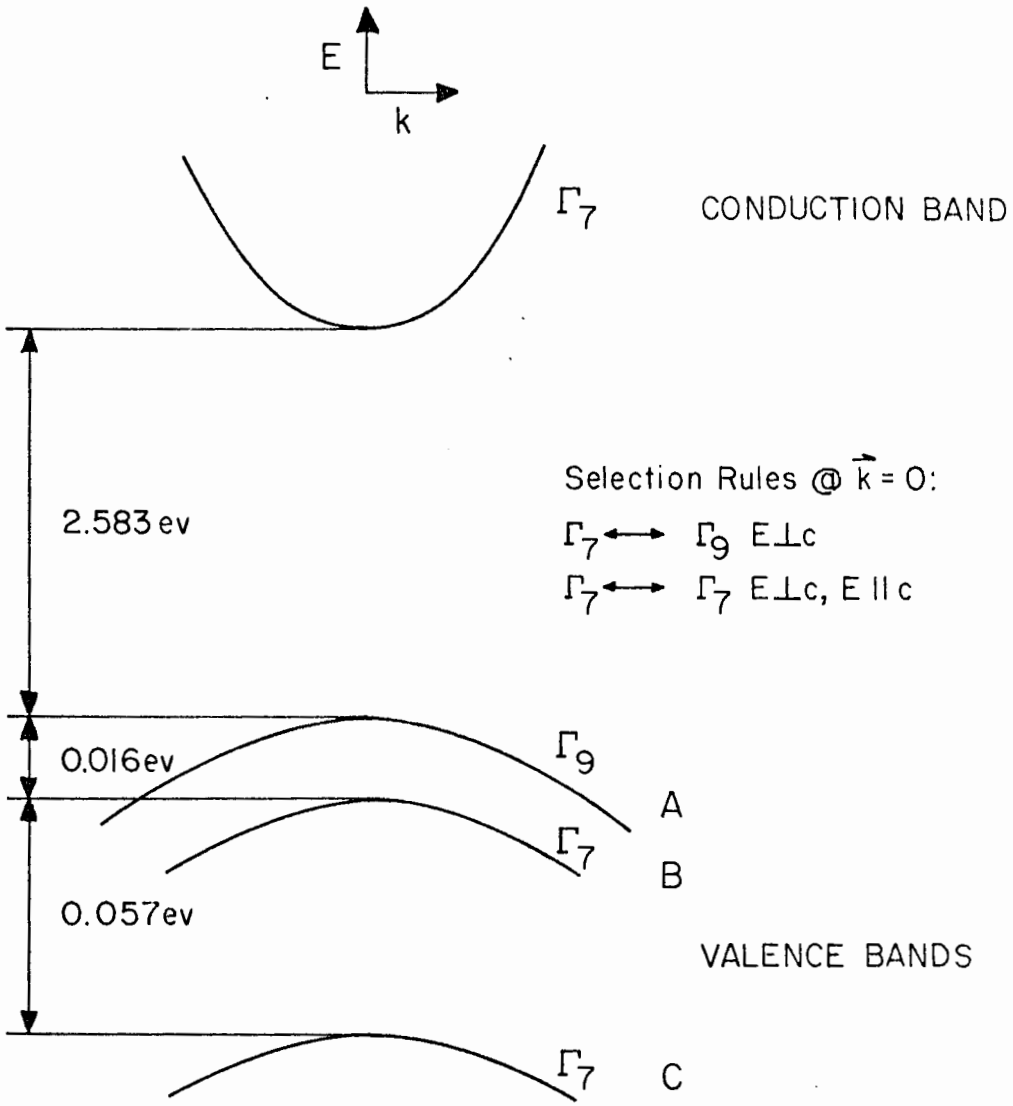

Fig. 1 Energy band configuration of CdS at $\vec{k}$=0, after Thomas and Hopfield (1959). The valence bands are labelled A, B and C and the irreducible representation of the $\vec{k}$=0 crystal double group to which each band belongs is indicated.

Table I. Intrinsic Excitons in CdS

Line	Position Å	eV*	Absorption or Luminescence	Polarization	Binding Energy	Reference
$A(1s_{\Gamma_6})$	4857.1	2.55193	a,ℓ	E||c		Hopfield and Thomas (1961)
$A(1s_{T\Gamma_5})$	4854.8	2.55314	a,ℓ	E⊥c	29.8 meV	" "
$A(1s_{L\Gamma_5})$	4852.9	2.55414	a			" "
$A(n=2, p_o)$	4814.2	2.57467	a	E||c	7.5	" "
$A(n=2, s_L)$ } $A(n=2, p_{\pm 1})$	4812.9	2.5737	a,ℓ	both	6.9	" "
A(n=3)	4805.5	2.5733	a		2.8	" "
A(n=4)	4803.3	2.58052	a		1.7	" "
B(n=1)	4826.1	2.56833	a,ℓ	both	29.5	" "
B(n=2)	4784.9	2.59044	a	both		" "
C	4710	2.632	a	both	26	Thomas and Hopfield (1959)

* Evaluated using $\frac{hc}{n} = 1.2395 \times 10^{-4}$cm eV, where n is the index of refraction of air at 15°C and 76 cm of Hg, in the wavelength region 4800-5100 Å. (CRC Handbook of Physics and Chemistry, 1972-73 edition).

Hopfield and Thomas apparently used an idex of 1 and slightly different values for the fundamental constants.

which requires some explanation. The 1s hydrogenic state of the A exciton may belong to either the Γ_5 (allowed transition at $\vec{k}=0$) or Γ_6 (forbidden) irreducible representation of the $\vec{k}=0$ group. The $A(\Gamma_5)$ exciton, which has electron and hole spins antiparallel, is observed for $\vec{E} \perp c$ as a transverse exciton (subscript T) and for $\vec{E} \| c$ as a weak longitudinal exciton (subscript L). The terms transverse and longitudinal refer to the two cases where the polarization field $\vec{P}$ of the exciton is perpendicular and parallel, respectively, to the exciton wave vector (see Hopfield and Thomas 1959). In CdS the longitudinal mode is weakly excited due to a coupling with the allowed transverse Γ_5 transition. The $A(\Gamma_6)$ exciton, which has electron and hole spins parallel, is forbidden at $\vec{k}=0$ but may be observed since photons have finite momentum. Due to the anisotropy of the effective mass for directions $\perp$ and $\|$ to the c axis, the degeneracy of the A(2p) exciton state is partially lifted. The subscripts $0, \pm 1$ refer to the number of units of orbital angular momentum about the c axis.

2.2. Bound Excitons in CdS

Free excitons may become localized at impurities to form bound complexes which are crudely analogous to the Hydrogen molecules H_2 and H_2^+. These complexes have lifetimes of the order of 10^{-9} sec. (Henry and Nassau, 1970a), and decay via

the emission of a photon when a constituent electron and hole recombine. The impurity is then left in either its ground state (one-electron transition) or in some excited state (two-electron transition). At low temperatures bound exciton emission is the most dominant feature of the luminescent spectrum. This is clearly illustrated in Fig. 2, a typical photoluminescent spectrum of a high purity crystal at 5.5°K. Although the crystal was not intentionally doped, it contained enough impurities to give strong bound exciton emission. The most intense line, labelled I_2, is due to an A exciton bound to a neutral donor (Cl in this case), and may be schematically represented by $\oplus^{-}_{-}+$. In this notation $\oplus$ refers to the fixed donor core, + and - represent a hole and an electron, respectively. The line labelled I_3 is due to an A exciton bound to an ionized donor and is represented as $\oplus^{-}+$. I_1 refers to an A exciton bound to a neutral acceptor and is represented by $\ominus^{+}_{+}-$. Hopfield (1964) has shown that an exciton is not bound to an ionized acceptor in CdS, due to the fact that the electron/hole effective mass ratio is too small (i.e. the electron is too light) for bound states of the electron to exist near a neutral acceptor (cf. the binding of a particle to a three dimensional square well).

The above classification of bound exciton complexes was first made in a classic paper by Thomas and Hopfield (1962). Their conclusions were drawn from a careful analysis of Zeeman

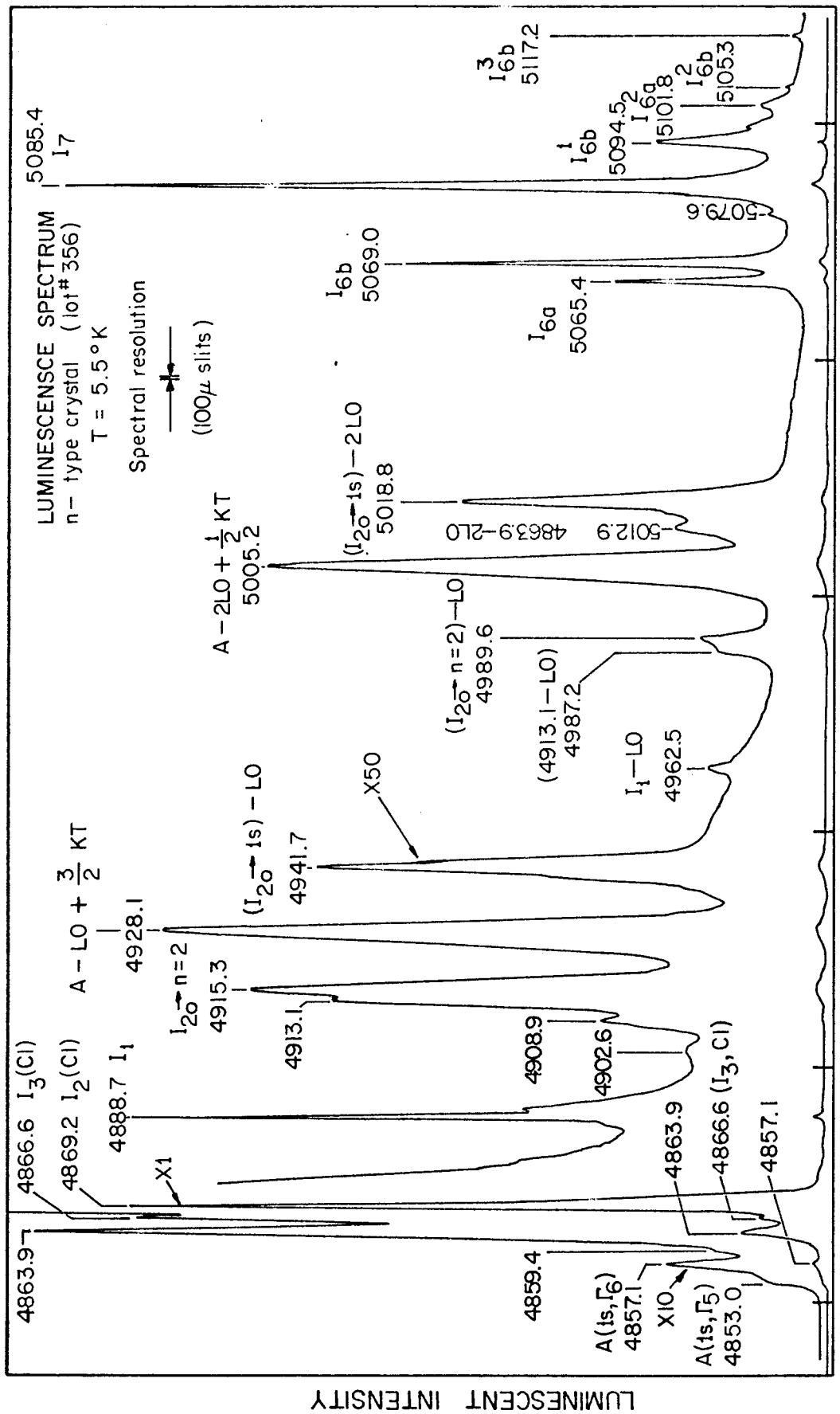

Fig. 2 Luminescence from a lightly doped CdS crystal at T = 5.5°K. The crystal was excited with above band-gap light provided by a Hg arc lamp. The transition at 4869.2Å will be subsequently labelled $I_{2o} \rightarrow 1s$ (see section 4).

splitting of the bound exciton lines. The exact wavelength of bound exciton emission depends on the particular impurity involved. Work by Nassau, Henry and Shiever (1970), and Henry, Nassau and Shiever (1970) has made possible the identification of many of the common donors and acceptors involved in bound exciton emission. Table II lists most of the known bound exciton lines along with the corresponding chemical impurity. The binding energies of the A exciton to each impurity is also given.

It is reasonable to describe weakly bound exciton states as though they belonged to the point group of the crystal rather than the point group of the impurity (Thomas and Hopfield 1962). This means that the selection rules governing bound exciton transitions are primarily determined by the corresponding band-to-band selection rules. Thus, the lines I_1, I_2 and I_3 are active mainly for $\vec{E} \perp c$ since the holes are from the A valence band. The absorption lines listed at the bottom of Table II, however, are active for both polarizations. Thomas and Hopfield (1962) identified these lines as follows. I_{2B} results from the creation of a B exciton bound to a neutral donor. I_{1B} and $I_{1B'}$ result from a B exciton bound to a neutral acceptor, with the hole spins being antiparallel and parallel, respectively. These lines are not observed as luminescent transitions because of rapid relaxation of the holes from the B to the A valence band.

Table II. Bound Excitons in CdS

Line	Position Å	Position ev	Chemical Impurity*	Binding Energy of A Exciton	Polarization	Reference**
LUMINESCENCE AND ABSORPTION						
I_{1a}	4888.5	2.53546	Li a	17.6 meV	$E \perp c$	i
I_{1b}	4888.2	2.53562	Na a	17.4	"	i
I_2	4870.6	2.54479	F d	8.25	"	ii
	4869.9	2.54515	In d	7.89	"	ii
	4869.2	2.54548	Cl d	7.58	"	ii
	4868.9	2.54565	I d	7.39	"	ii
	4867.1	2.54661	$[Li\ d]^+$	6.5	"	iii,iv
I_3	4870.3	2.54495	F id	8.09	"	ii
	4866.6	2.54686	Cl id	6.20	"	ii
	4865.8	2.54729	I id	5.75	"	ii
	4861.7	2.54943	$[Li\ id]^+$		"	iii,iv
I_6 zero field split	5068.5	2.4454	?		$E \parallel c$	v
	5069.2	2.4451	?		$E \parallel c$	v
I_7	5084.8	2.43758	?		both	v

.../continued

Table II - Continued from Page 10

ABSORPTION ONLY				Binding Energy of B Exciton		
I_{1B}	4863.7	2.54839		19.8 meV	E||c	iv
	4863.2	2.54865	Li or Na		E⊥c	iv
$I_{1B'}$	4860.8	2.54991		18.3	E||c	iv
I_{2B}	4837.7	2.56209	$[Li\ \ d]^{+}$	6.2	both	iv

* a - neutral acceptor; d - neutral donor; id - ionized donor.

\+ tentative assignment. ** i Henry, Nassau and Shiever (1970)

ii Nassau, Henry and Shiever (1970)

iii Malm (1971)

iv Thomas and Hopfield (1962)

v Reynolds and Litton (1963)

Many of the lines appearing at longer wavelengths in Fig.2 occur at intervals of one or two LO phonon energies below strong transitions such as the intrinsic A exciton and the I_1 and I_2 bound excitons. These lines are usually referred to as LO phonon replicas. Indeed, LO phonon coupling is a common feature of almost all luminescence in CdS.

2.3 Long Wavelength Bound Exciton Emission in CdS

The lines labeled I_6 (zero field split) and I_7 in Table II were reported by Reynolds and Litton (1963). These transitions were observed primarily in n-type crystals (I_1 very weak) but were also seen in some compensated crystals ($I_1 \approx I_2$). The magnetic properties of I_6 and I_7 were investigated but only I_6 displayed any Zeeman effect. The 5068 Å component of I_6 was isotropically split for different orientations of the magnetic field, with the amount of splitting increasing non-linearly with increasing field strength ($H||c$). The 5069 Å component also seemed to split, but for some reason one of the magnetically split components was not observed. In zero field the components of I_6 were of equal intensity. The similarity of the zero field splitting of I_6 to that of the I_3 transition led Reynolds and Litton (1963) to suggest that the I_6 line was due to the decay of an exciton bound to an ionized center. Since this time, no further work has been

reported on these long wavelength lines.

2.4 Physical Constants for CdS

Those physical parameters of CdS which are pertinent to this thesis are listed in Table III. A more extensive list is available in II-VI Semiconducting Compounds Data Tables compiled by Neuberger (1969).

2.5 A Radiative Auger Process

The Auger process, as a nonradiative recombination mechanism in semiconductors, has been known for some time (for example, see Peierls 1932). In the nonradiative Auger process the energy released by a recombining electron and hole is absorbed by another electron, which then dissipates the energy by emission of phonons. Thus the Auger process is, by definition, a three-body interaction.

Since the I_2 bound exciton is essentially a three-body complex, the Auger process is a possible mechanism for its decay. The nonradiative Auger process in this case involves collapse of the exciton by nonradiative recombination of the hole with a constituent electron, and simultaneous promotion of the remaining donor electron deep into the conduction band. This nonradiative Auger effect was once postulated as a "killer mechanism" for radiative bound exciton decay,

Table III. Measured Parameters of CdS

		Reference
Effective mass in terms of the free electron mass	$m_{e\perp} = .190 \pm .002$	Henry and Nassau (1970b)
	$m_{e\parallel} = .180 \pm .010$	
	$m_{h\perp} = 0.7 \pm 0.1$	Thomas and Hopfield (1959)
	$m_{h\parallel} = 5.0$	
Dielectric constant		
- static κ_s	$\kappa_{\parallel} = 9.48$	Berlincourt et al.
(77°K)	$\kappa_{\perp} = 8.48$	(1963)
Refractive index		
($\kappa_o = n^2$)	$n = 2.29 = (5.24)^{\frac{1}{2}}$	Czyzak et al. (1957)
Phonon energies	LO(Γ_1) 305 cm^{-1}	Tell, Damen and
(Raman Scattering)	LO(Γ_5) 305 cm^{-1}	Porto (1965)

resulting in low efficiencies for I_1 and I_2 emission even at low temperatures (Shinonoya 1970). Recent measurements of the radiative lifetimes of bound excitons in CdS by Henry and Nassau (1970a), however, indicate that the Auger effect is negligible for I_1 and I_2 compared with radiative decay.

The discrete two-electron transitions mentioned in section 1 are a form of Radiative Auger process. In this case the energy from the electron-hole recombination is divided between an emitted photon and the residual electron, which is projected onto an excited bound state of the neutral donor. Discrete luminescent lines result due to the discreteness of the hydrogenic donor states. The existence of a luminescent Auger band in CdS has been indicated by the experimental results of Malm and Haering (1971a). This process again involves energy sharing between an emitted photon and the residual electron, but in this case the electron is promoted into the conduction band. A luminescent band results since the final states of the residual electron form a continuum. Due to the fact that this mechanism creates free carriers, it is of some consequence in the interpretation of photoconductivity data.

2.6 Isoelectronic Traps

An isoelectronic trap is a substitutional impurity which is from the same column of the periodic table as the host atom it replaces. If the electronegativity difference between the

host and impurity atoms is large, the center may bind an electron or hole (depending upon the sign of the electronegativity difference) by a strong short-range interaction. The resulting charged center can then bind the oppositely-charged particle through a long-range coulomb interaction, to form a bound exciton complex. If the primary particle is an electron, the center is called an isoelectronic acceptor since it can then bind a hole. Similarly, if the primary particle is a hole, an isoelectronic donor results. Known examples of isoelectronic traps are Te substituting for S in CdS, N or Bi substituting for P in GaP, and O substituting for Te in ZnTe (Hopfield, Thomas and Lynch, 1966).

Since the bound exciton complexes formed by isoelectronic traps are essentially two particle systems, Auger recombination is not a likely mechanism for decay. This, together with the large binding energies which are about 100mev to 400mev for the above centers, can result in strong luminescence even at high temperatures.

2.7 Deep Donors and Acceptors

It is well known that certain impurities form deep centers in some semiconductors. For example, Phosporous and Arsenic form acceptors in CdS at about 1 ev above the valence band (Tell 1970), and Copper forms acceptor levels at 180 and

410 mev, as well as a donor level at 70mev in GaAs (Morgan, Pilkuhn and Rupprecht 1965). In some cases the addition of these centers produces broad band luminescence, generally well below the band-gap. Although the nature of such emission is now better understood (see Shionoya 1970), little is known about the actual electronic structure of the deep impurities involved. In particular, the existence of excitons bound to deep donors and acceptors has not been described theoretically, or been reported experimentally, with the possible exception of the I_6 and I_7 lines reported by Reynolds and Litton (1963).

3. Experimental Techniques and Apparatus

3.1 Optical System

Three main types of optical experiments were performed:

(i) Above band-gap excitation

The sample was excited with above band-gap radiation provided either by the blue and violet lines of a 100 watt Hg arc lamp, selected by a band-pass filter; or by one of the blue lines of an Argon-ion laser. This type of excitation creates free electrons and holes which may recombine radiatively by cascading through the various available luminescent centers. In this way virtually all the luminescent lines of the sample are excited. A high resolution grating spectrometer was used to analyze the luminescence.

(ii) Selective excitation

By means of a monochromator, the wavelength of the exciting light was chosen to coincide with an absorption line of a luminescent center. A spectrum of the emission at lower energies, taken by the analyzing spectrometer, then indicated which transitions were associated with the excited line. In this way a complex spectrum may often be simplified by grouping those lines which are related to a given complex.

(iii) Selective Luminescence

The analyzing spectrometer was used to select a particular

luminescent line. The monochromator was then used to sweep the wavelength of the incident light at higher energies. A recording of the luminescent intensity of the selected transition vs. wavelength of the exciting light is called the excitation spectrum of the chosen luminescent line. Excitation spectra have been used by Malm and Haering (1971a) to observe excited states of the I_2 bound exciton complex in CdS.

The configuration of the optical system for experimental modes (ii) and (iii) is shown schematically in Fig. 3(a). The monochromator was a Spex Industries Model 1700 and had an average linear dispersion of 5 Å/mm in second order. For all experiments 200 micron slits were used, corresponding to a bandwidth of about 1 Å for the exciting light. The source, a 100 Watt Mercury arc lamp, was focused onto the incident slit of the monochromator so as to fully illuminate the grating. This condition is met when the f-number of the focusing optics matches that of the monochromator (f-6.8).

That part of the emission spectrum of the Hg arc lamp which was used in modes (ii) and (iii) above, is shown in Fig. 3(b). Since the lamps used had little flicker and reasonably constant intensity of emission in wavelength regions of interest, a technique for correcting incident intensities, due to Conradi (1968), was not used.

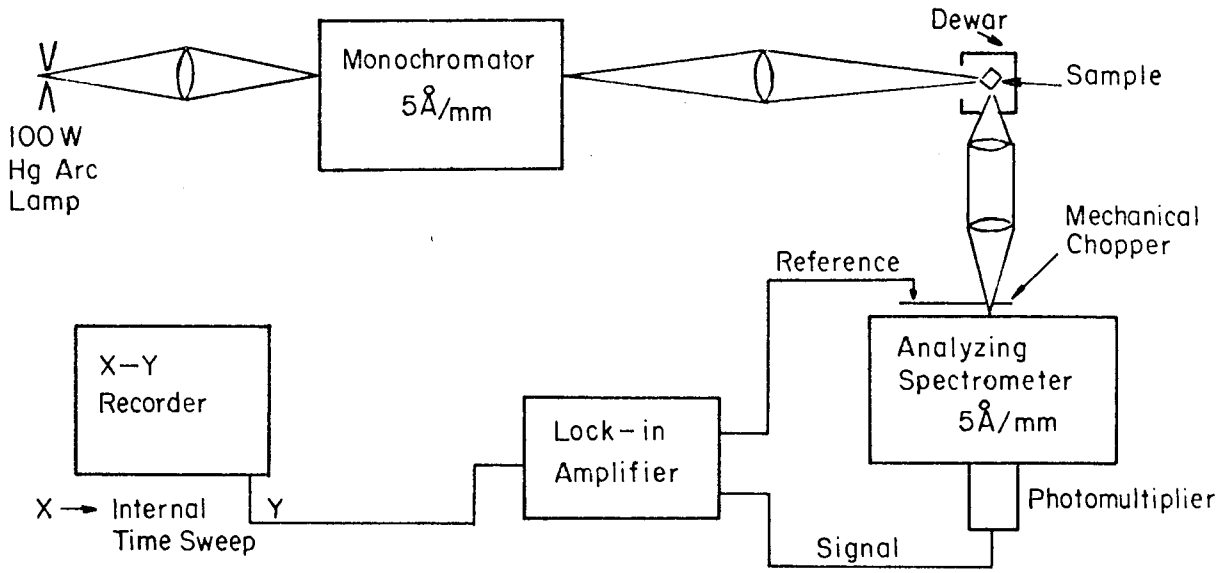

(a)

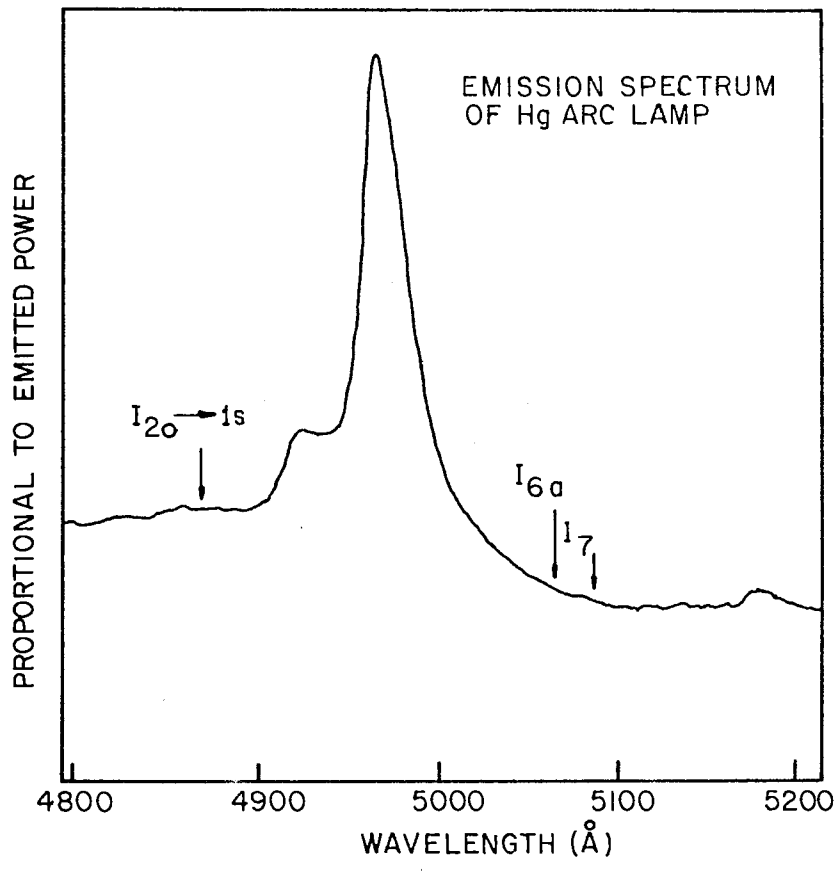

(b)

Fig. 3 (a) Schematic of experimental apparatus for optical excitation. (b) Spectrum of high pressure Hg arc source. The approximate positions of some important luminescent lines are indicated.

A high quality camera lens (f-1.4) of focal length 50mm was used to focus the incident light onto the crystal, via a small mirror mounted on the sample holder. The mirror reflected the focused light onto the crystal in such a way as to minimize the specular reflection of exciting light into the collection optics. This precaution illiminates stray lines due to grating ghosts produced by the exciting light, and is very important when analyzing weak luminescent transitions.

The luminescent light from the crystal was collected with a 55 mm, f-1.2 camera lens. A high quality small focal length, small f-number lens was required for this purpose to cover as much of the solid angle subtended at the crystal as possible. This was extremely important for modes (ii) and (iii) since the crystal was only weakly excited (with 1000 micron slits the monochromator only provides about 0.05 mw at 4800 Å). The luminescent light was collimated by the collecting lens and then focused, by means of a second lens, onto the entrance slit of a Spex Industries Model 1702 spectrometer. As with the monochromator, care was taken to match the f-number of the spectrometer so that the grating would be fully illuminated. The linear dispersion of the spectrometer was 5Å/mm in second order. In experimental modes (ii) and (iii), 200 micron slits were used, corresponding to a spectral

resolution of about 1Å. For mode (i), either 100 or 50 micron slits were used corresponding to resolutions of 0.5 and 0.25Å, respectively.

At the exit slit of the spectrometer, a small lens was used to focus the exciting light onto the photocathode of a high sensitivity ITT FW130 photomultiplier (S-20 response). This lens was necessary since the FW130 has a very small effective cathode diameter, about 2.5mm. In order to reduce noise due to dark current, the photomultiplier was cooled with a dry ice - alcohol slurry. The light entering the spectrometer was mechanically chopped at 80 Hz, and the photomultiplier signal was analyzed by means of a lock-in amplifier.

3.2 Cryostat

The experiments were performed with a variable temperature, stainless-steel dewar manufactured by Andonian Associates Inc.. The samples were mounted on a copper block and maintained in a He gas environment at about one atmosphere. Temperature variation was achieved by means of controlling the flow of cold He gas ambient, and the flow of current to a sample heater. A Au-0.03% (at. wt.) Fe vs. Chromel thermocouple* was used to measure the temperature, which, for the different experiments, varied from 4.2°K to 115°K.

---

* Kindly provided by Prof. D. J. Huntley, Simon Fraser University.

3.3 Sample Preparation

All CdS samples used in the experiments were of ultra-high purity (UHP) grade, purchased from Eagle-Picher. These crystals were n-type, the donor being identified as Chlorine from luminescent spectra. The donor concentrations were $\sim 10^{15}/cm^3$, estimated from conductivity measurements** in the temperature region of impurity saturation ($\sim$100°K). It was necessary to use high purity crystals in order to observe the luminescent features studied, namely the two-electron transitions and the I_6 and I_7 lines. (The I_6 and I_7 transitions may also be observed in some compensated crystals, but their intensity is generally very weak compared to the intensity of the same lines in high purity samples).

Seven different lots of UHP crystals were used, with all crystals showing very strong I_2(Cl) transitions at low temperatures. All samples displayed the same set of long wavelength I_6 and I_7 exciton lines, but with different relative intensities. Lot #356 showed the strongest long wavelength lines, and also proved satisfactory for observing the two-electron transitions.

The crystals were either cleaved, or etched in concentrated HCl, with the c-axis lying in the plane of the prepared

---

** Measurements performed by R. M. Egloff, Simon Fraser University.

surface. The etching time was from 30 to 60 secs., followed by a thorough washing in distilled water. Samples were mounted with a small dab of nail polish, applied at one end only to reduce strain. Since prolonged exposure of a freshly cleaved or etched sample to air reduces luminescent efficiency, sample preparation time was limited to a few minutes, and crystals were maintained in a He atmosphere immediately after mounting.

PART I - RADIATIVE DECAY OF THE I_2 COMPLEX (Exciton bound to a neutral donor)

4. Radiative Decay of the I_2 Complex - Theory

When the hole recombines with one of the electrons to collapse the I_2 complex, the remaining electron will be projected either onto a bound state of the neutral donor, or an unbound coulomb state of the ionized donor core. The former process results in discrete luminescent lines, the latter produces a luminescent Auger band. If the I_2 complex is in its lowest energy configuration, the transition to the ground or 1s hydrogenic state of the neutral donor results in the dominant luminescent line at 4869.2Å (Cl donor) in Fig. 2. (Transitions from excited states of the I_2 complex also occur - Malm and Haering 1971a, but need not be considered for what follows). This line will henceforth be referred to as the $I_{2o} \rightarrow 1s$ transition. (The subscript o refers to the ground state of the I_2 complex). Its large relative intensity indicates that the residual electron has the greatest probability of being left in the 1s hydrogenic state. There is finite probability, however, that the remaining electron will be excited to higher energy levels (2s, 2p, 3s etc.) of the neutral donor. Such transitions are referred to as two-electron transitions, and will result in luminescent emission lower in energy than the $I_{2o} \rightarrow 1s$ transition by amounts equal

to the energies of the excited hydrogenic levels. Fig. 4(a) is a sketch of the energy level diagram for the $I_{2o} \rightarrow 1s$ and two-electron transitions. The luminescence from these transitions is represented schematically in Fig. 4(b). Thus, as we move from the bottom of Fig. 4(b) toward the top (or from left to right in Fig. 4(a)), the observed two-electron lines represent more and more energy being given to the electron remaining on the neutral donor, until a point is reached - at the edge of the broad band in Fig. 4(b) - where the electron is ionized. This is the radiative Auger band discussed in section 2.5. It represents the extension of the two-electron transitions to the unbound coulomb states of the positive donor core.

4.1 Application of the Sudden Approximation

In the center of mass frame of the nucleus (assumed fixed), let the three particle wave function describing the bound exciton in its lowest energy configuration be:

$$\Psi(\vec{r}_1, \vec{r}_2, \vec{r}_h) \qquad 4.1.1$$

where $\vec{r}_1$, $\vec{r}_2$ and $\vec{r}_h$ are the coordinates of the two electrons and the hole, respectively. In a manner similar to the treatment of shallow donor states (see Kohn 1953) we may consider 4.1.1 to be an exciton envelope function. Thus the total wave function may be approximated by the product of 4.1.1 and

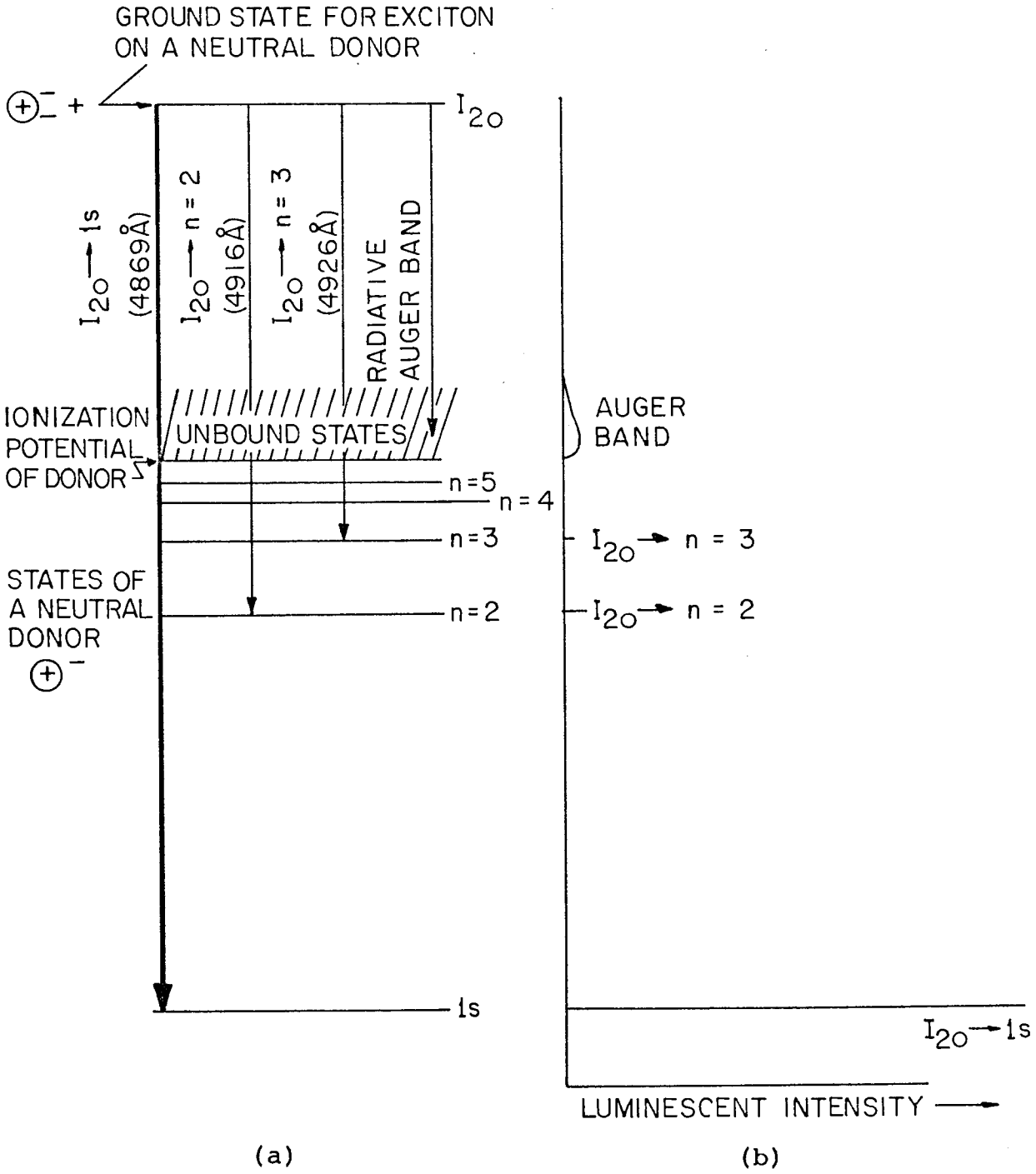

Fig. 4 (a) Energy levels for the $I_{2o} \rightarrow 1s$ and two-electron transitions. The wavelengths indicated are those for the Cl donor in CdS. (b) Schematic of resulting luminescence.

three zone center Bloch functions corresponding to the two electrons and a hole. Neglecting anisotropies, the effective mass Hamiltonian for the bound exciton complex may be written in the form:

$$H = -\frac{\hbar^2}{2}\left(\frac{\nabla_1^2}{m_1^*}+\frac{\nabla_2^2}{m_2^*}+\frac{\nabla_h^2}{m_h^*}\right) - \frac{e^2}{\kappa}\left(\frac{1}{|\vec{r}_1|}+\frac{1}{|\vec{r}_2|}-\frac{1}{|\vec{r}_h|}\right)$$

$$+\frac{e^2}{\kappa}\frac{1}{|\vec{r}_1-\vec{r}_2|} - \frac{e^2}{\kappa}\frac{1}{|\vec{r}_1-\vec{r}_h|} - \frac{e^2}{\kappa}\frac{1}{|\vec{r}_2-\vec{r}_h|} + H'(t) \qquad 4.1.2$$

$$= H_o + H'(t) \qquad 4.1.3$$

where m_i^* is the average effective mass of particle i and κ is the average static dielectric constant. $\Psi(\vec{r}_1,\vec{r}_2,\vec{r}_h)$ will be an eigenfunction of H_o. $H'(t)$ is the time dependent part of the Hamiltonian which induces the collapse of the exciton. Let us assume that we may extract that part of the wave-function which describes a single electron. This is a simple matter if $\Psi(\vec{r}_1,\vec{r}_2,\vec{r}_h)$ can be written as a product of single particle wave functions. Even in a more general case, however, we shall assume that a single particle wave function may be extracted by integration of the total wave function:

$$\varphi(\vec{r}_1) \equiv \int \Psi(\vec{r}_1,\vec{r}_2,\vec{r}_h)\,d\vec{r}_2 d\vec{r}_h \qquad 4.1.4$$

$\varphi(\vec{r}_1)$ will be an approximate eigenfunction of an effective

one-electron Hamiltonian defined by

$$H_{eff} \equiv \frac{-\hbar^2}{2m_1^*}\nabla_1^2 - \frac{e^2}{\kappa|\vec{r}_1|} + \frac{e^2}{\kappa}\left\langle\frac{1}{|\vec{r}_1-\vec{r}_2|}\right\rangle_{AV} - \frac{e^2}{\kappa}\left\langle\frac{1}{|\vec{r}_1-\vec{r}_h|}\right\rangle_{AV} \qquad 4.1.5$$

where

$$\langle f(\vec{r}_1,\vec{r}_2,\vec{r}_h)\rangle_{AV} \equiv \int\psi^*(\vec{r}_1,\vec{r}_2,\vec{r}_h)f(\vec{r}_1,\vec{r}_2,\vec{r}_h) \times\psi(\vec{r}_1,\vec{r}_2,\vec{r}_h)d\vec{r}_2 d\vec{r}_h \qquad 4.1.6$$

Thus we have defined a one-electron bound state, in the presence of the exciton complex, such that the eqn.

$$H_{eff}\varphi(\vec{r}_1) = E_{eff}\,\varphi(\vec{r}_1) \qquad 4.1.7$$

is reasonably valid. Equation (4.1.7) is the Hartree approximation.

Consider that at t=0 the exciton collapses. For t>0, the residual electron will be in some bound hydrogenic state of the neutral donor, or in an unbound coulomb state. The Hamiltonian for the residual electron may be written:

$$H_e = \begin{cases} H_{eff} & t < 0 \\ H_{donor} & t > 0 \end{cases} \qquad 4.1.8$$

where

$$H_{donor} = \frac{-\hbar^2}{2m_1^*} \nabla_1^2 - \frac{e^2}{\kappa|\vec{r}_1|} \qquad 4.1.9$$

Thus the Hamiltonian changes discontinously at t=0.

The wavefunction $\varphi'(\vec{r}_1)$ of the electron for t>0 may be expanded in terms of the eigenfunctions of the Hamiltonian in eqn. 4.1.9:

$$\varphi'(\vec{r}_1) = \sum_{n,\ell} a_{n\ell}\phi_{n\ell}(\vec{r}_1) + \int F(\vec{k})F_\ell(\vec{k},\vec{r}_1)d^3\vec{k} \qquad 4.1.10$$

where $\phi_{n\ell}(\vec{r}_1)$ are the radial parts of the hydrogenic wavefunctions and $F_\ell(\vec{k},\vec{r}_1)$ are coulomb wavefunctions (Abramowitz and Stegun 1968). Thus the functions $\phi_{n\ell}(\vec{r}_1)$ represent the bound states of the neutral donor and the functions $F_\ell(\vec{k},\vec{r}_1)$ represent the unbound continuum states. The probability of observing a particular state is given by the modulus squared of its expansion coefficient, i.e. $|a_{n\ell}|^2$ is the probability of observing the state $\phi_{n\ell}(\vec{r}_1)$, $|F(\vec{k})|^2$ is the probability of observing the state $F_\ell(\vec{k},\vec{r}_1)$.

Since the time dependent Schrodinger equation is first order in time, the electron wavefunction must be continuous as a function of time, even though its first derivative is not. Thus we must have at t=0

$$\varphi(\vec{r}_1) = \varphi'(\vec{r}_1) \qquad 4.1.11$$

or

$$\varphi(\vec{r}_1) = \sum_{n,\ell} a_{n\ell}\phi_{n\ell}(\vec{r}_1) + \int F(\vec{k}) F_\ell(\vec{k},\vec{r}_1) d^3\vec{k} \qquad 4.1.12$$

from eqn. 4.1.10.

In physical situations where the Hamiltonian suffers a sudden transition requiring a finite amount of time, the use of condition 4.1.11 is called the Sudden Approximation (Schiff 1968). It means that the Hamiltonian changes much faster than characteristic times required for physical adjustment of the system's wavefunction. The initial wavefunction is then projected directly onto the final states as in eqn. 4.1.12. The Sudden Approximation has been applied to such situations as Beta decay (Bohm 1951) and sudden reversal of magnetic fields (Messiah 1966).

The use of the term Sudden Approximation to describe the process of obtaining eqn. 4.1.12 requires some comment. In the context of bound exciton decay this title is not strictly correct since we cannot define any "characteristic time" for the transition of the Hamiltonian. The change is produced by the collapse of the exciton, which is instantaneous. The only approximation lies in assuming we can define one-electron bound states in the presence of the exciton complex, as in eqn. 4.1.7. The term Sudden Approximation is useful, however, since it implies the use of condition 4.1.11.

4.2 Projection onto the Bound States (Discrete Luminescent Lines)

Assuming that the complete set of eigenfunctions of H_{donor} (eqn. 4.1.9) have been orthogonalized, we may obtain from eqn. 4.1.12:

$$|a_{n\ell}|^2 = \left|\int \varphi(\vec{r}_1)\phi_{n\ell}(\vec{r}_1)d^3\vec{r}_1\right|^2 \qquad 4.2.1$$

Eqn. 4.2.1 indicates that the probability of observing a given hydrogenic state is equal to the modulus squared of the projection of $\varphi(\vec{r}_1)$ onto that state. Since the quantity on the righthand side of eqn. 4.2.1 is proportional to the intensity of the corresponding discrete two-electron transition, the coefficients $a_{n\ell}$ (aside from a possible phase factor) may be determined, in principle at least, from experimental data.

4.3 Projection onto the Unbound States (the Radiative Auger Band)

As mentioned previously, the Auger band, represented in Fig. 4(b), corresponds to the residual electron involved in a two-electron transition being promoted into the conduction band. In analogy with eqn. 4.2.1, the experimentally observed Auger band is essentially a measure of $|F(\vec{k})|^2$, where

$$|F(\vec{k})|^2 = \left|\int \varphi(\vec{r}_1)F_{\ell}(\vec{k},\vec{r},)d^3\vec{r}_1\right|^2 \qquad 4.3.1$$

Thus, since the form of the functions $\phi_{n\ell}(\vec{r}_1)$ and $F_\ell(\vec{k},\vec{r}_1)$ are well known, it should be possible, in principle, to determine the form of the electron wavefunction $\varphi(\vec{r}_1)$ in eqn. 4.1.10 from a detailed experimental knowledge of the relative intensities of the $I_{2o}\rightarrow 1s$, and two-electron transitions.

If we make use of a crude approximation - that the ionized electrons may be described by momentum eigenfunctions, $F(\vec{k})$ may be written in the form

$$F(\vec{k}) = \int \varphi(\vec{r}_1) e^{-i\vec{k}\cdot\vec{r}_1}\, d^3\vec{r}_1 \qquad 4.3.2$$

Eqn. 4.3.2 is the Fourier transform of $\varphi(\vec{r}_1)$ in momentum space. Inverting 4.3.2:

$$\varphi(\vec{r}_1) = \frac{1}{(2\pi)^3} \int e^{i\vec{k}\cdot\vec{r}_1}\, F(\vec{k}) d^3\vec{k} \qquad 4.3.3$$

Eqn. 4.3.3 represents an expansion of the single electron wavefunction in terms of momentum eigenfunctions. Although it is more correct to use coulomb wavefunctions, the Fourier transform behavior of eqn. 4.3.2 will prove useful in estimating the spatial extent of $\varphi(\vec{r}_1)$ (section 5.2).

5. Radiative Decay of the I_2 Complex - Experimental Results and Discussion

5.1 Projection onto the Bound States

The $I_{2o} \rightarrow 1s$ and $I_{2o} \rightarrow n=2$ two-electron transition, where the exciton collapses leaving the residual electron in the n=2 hydrogenic state of the neutral donor, are clearly visible at 4869.2Å and 4915.3Å (Cl donor) in Fig. 2, a spectrum taken in experimental mode (i). Certain weaker features of the two-electron transitions, however, are obscured by extraneous lines. This difficulty may be overcome by means of selective excitation (mode (ii)). In Fig. 5 the crystal was illuminated at the energy of the $I_{2o} \rightarrow 1s$ transition and a spectrum of the luminescence at lower energies was recorded. The luminescence due to other complexes has been suppressed and the two-electron processes are mapped out in more detail.

Due to crystal anisotropies, the degeneracy of the n=2 donor level is partially lifted. The lines at 4915.3Å and 4916.3Å are labelled $I_{2o} \rightarrow 2s$, and $I_{20} \rightarrow 2p_x$, $2p_y$ after Henry and Nassau (1970b). The subscript o implies that decay is from the ground state of the exciton complex as before, and the subscripts x and y refer to directions $\perp$ to the c-axis (z direction). The transition $I_{2o} \rightarrow 2p_z$ is not observed.

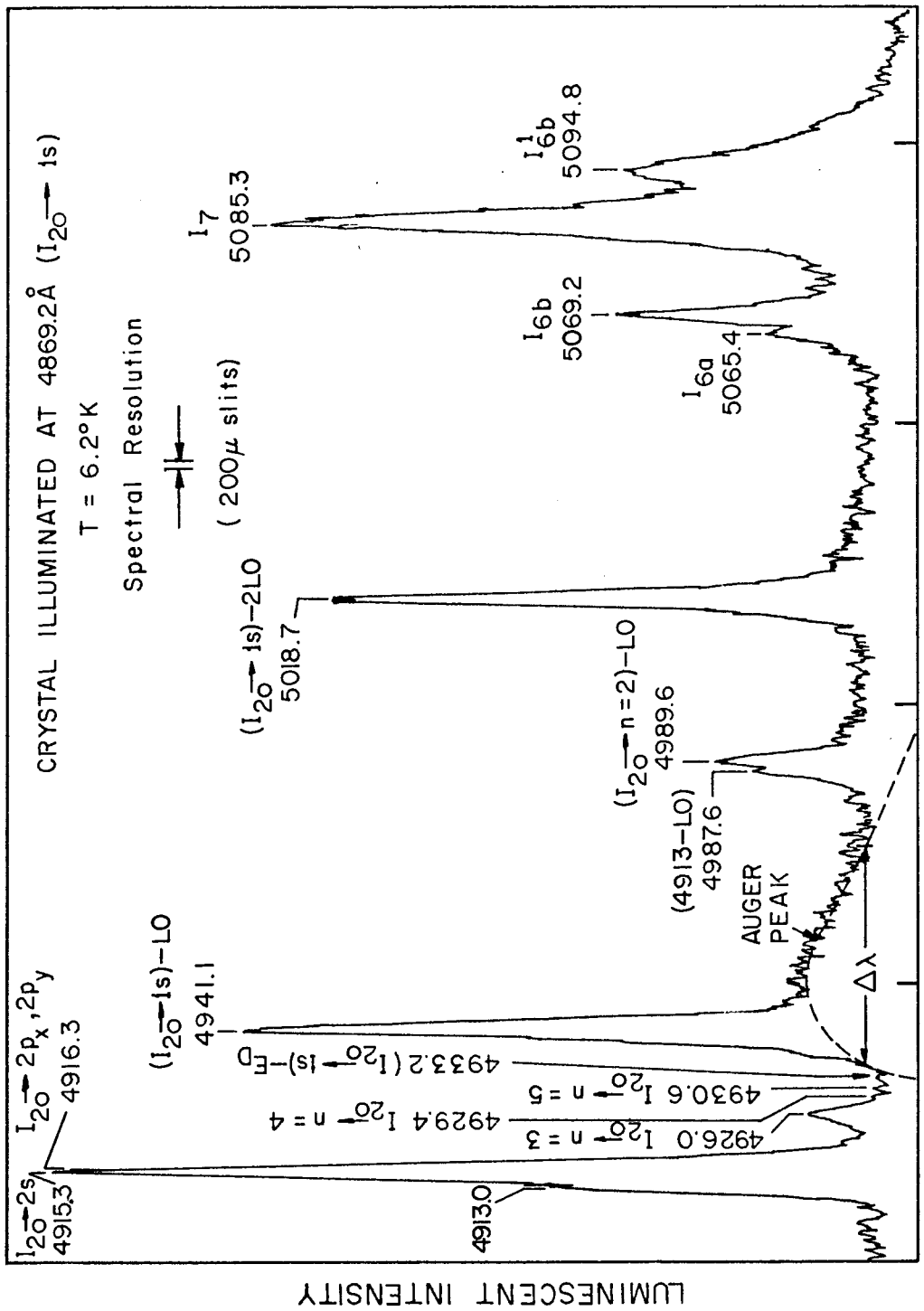

Fig. 5 Luminescent spectrum of a crystal excited at 4869.2Å, the I_{2O}→1s transition.

The weak transition $I_{2o} \rightarrow n=3$ at 4926Å is always visible, but much weaker transitions, corresponding to the observation of n=4, n=5 etc. levels, are difficult to observe since the signal to noise ratio is $\lesssim 1$ for these lines. Peaks at 4929.4Å and 4930.6Å have been tentatively identified as $I_{2o} \rightarrow n=4$ and $I_{2o} \rightarrow n=5$, respectively. This assignment is subject to some doubt due to the level of noise in the spectrum, but correlations with similar spectra indicate that these lines are probably real.

Energies of the hydrogenic states of the Cl donor in CdS, calculated from the present data, are presented in Table IV and compared with the results of Henry and Nassau (1970b) and Malm and Haering (1971a). Using the experimentally determined value of the donor ionization potential, corresponding energies for the hydrogen model have been calculated, without central cell correction, and are presented for comparison.

The data available from our results is not accurate enough to provide an expansion for the electron wave function $\varphi(\vec{r}_1)$ in terms of the hydrogenic states, as outlined in section 4.1. In particular, the distribution of the transition probability, from I_{2o} to the various wavefunctions belonging to a given principle quantum number, is not clear due to a lack of resolution. It is clear, however, from equation 4.1.12 and the relative intensity of the $I_{2o} \rightarrow 1s$ transition in Fig. 2, that the donor electron wavefunction is strongly

Table IV - Hydrogenic States of a Cl Donor in CdS

Hydrogenic Level	Present Results mev	Henry and Nassau (1970b) mev	Malm and Haering (1971a) mev	Hydrogen Model (no corrections) mev
1s	0	0	0	0
2s	23.87±0.05	23.88±0.02	23.8±0.05	
$2p_z$		24.19 "	24.2 "	24.75
$2p_x, 2p_y$	24.37 "	24.36 "	24.4 "	
n = 3	29.35 "		29.4±0.1	29.33
n = 4	31.09 "		31.5 "	30.94
n = 5	31.69 "		32.2 "	31.68
n = ∞	33±0.2	32.7±0.4	33.±0.2	33.0 (value from experiment)

1s-like in the presence to the exciton. This allows us to picture the ground or I_{2o} state of the bound exciton as having one electron bound to the donor core in a 1s-like orbital, and the other electron as bound to the hole to form an exciton. Such a model was shown by Henry and Nassau (1970a) to yield a reasonable value for the lifetime of the $I_{2o} \rightarrow 1s$ line.

This result suggests a possible trial wavefunction for the bound exciton ground state. Choosing the origin at the center of mass of the donor core, let $\vec{r}_1$, $\vec{r}_2$, $\vec{r}_h$ be the coordinates of the two electrons and hole. We assume that one electron is in a 1s hydrogenic state $\Psi_{100}(\vec{r}_1, \theta, \phi)$ about the donor. Introducing relative and center of mass coordinates for the second electron and hole:

$$\vec{r} \equiv \vec{r}_2 - \vec{r}_h \qquad \vec{R} \equiv \frac{m_e^* \vec{r}_2 + m_h^* \vec{r}_h}{m_e^* + m_h^*}$$

;

$$\frac{1}{\mu} = \frac{1}{m_e^*} + \frac{1}{m_h^*} \text{ (reduced mass)} \qquad M = m_e^* + m_h^*$$

We assume the excition is in a 1s-like hydrogenic state $\Psi'_{100}(\vec{r}, \theta', \phi')$ in the relative coordinates, and expand the wavefunction of the center of mass about the donor core in a suitable set of basis functions. Choosing these basis functions to be hydrogenic wavefunctions, the trial exciton

wavefunction has the form:

$$\Psi(\vec{r}_1,\vec{r},\vec{R},\theta,\phi,\theta',\phi')=\Psi_{100}(\vec{r}_1,\theta,\phi)\Psi'_{100}(\vec{r},\theta',\phi')\sum_{n\ell m} a_{n\ell m}\Psi_{n\ell m}(\vec{R},\theta,\phi)$$

Through the results of section 4.1 and experimental data regarding the exciton binding energy and two-electron transitions, it should be possible to determine the dominant terms in the above summation. Such an analysis, however, requires much more accurate data than is presently available.

5.2 Projection onto the Unbound States

As has been discussed in section 4.2, the Auger band in Fig. 5 represents a mapping of the donor wavefunction $\varphi(\vec{r}_1)$, in the presence of the I_2 complex, onto the unbound coulomb states of the donor core. Although partially obscured by the presence of an LO phonon replica of the $I_{2o}\rightarrow 1s$ transition, the shape of the Auger band is clear and has been indicated in Fig. 5. The wavelength spread $\Delta\lambda$ corresponds to an energy spread ΔE. If we assume a parabolic conduction band

$$E(k) = \frac{\hbar^2 k^2}{2m_e^*} \qquad 5.2.1$$

where $m_e \equiv (m_{e||}^* m_{e\perp}^*)^{\frac{1}{2}}$

then ΔE may be used to estimate the spread Δk in k-space of

the unbound states onto which the residual electron is projected. This is essentially the width of the function $F(\vec{k})$ in eqn. 4.3.2. Since $\varphi(\vec{r}_1)$ is the Fourier Transform of $F(\vec{k})$ (see eqn. 4.3.3), the spatial extent Δr of $\varphi(\vec{r}_1)$ is related to Δk by the approximate relation

$$\Delta r \Delta k \sim 1 \qquad 5.2.2$$

Using the above analysis, we find

$$\Delta r \approx 43 \pm 5 \text{ Å} \qquad 5.2.3$$

From the experimentally determined value of the donor binding energy E_D (see Table IV), we may calculate the effective Bohr radius of the Cl donor from the relation

$$a^* = \frac{e^2}{2\kappa E_D} \qquad 5.2.4$$

where $\kappa \equiv (\kappa_{||}\kappa_{\perp})^{\frac{1}{2}}$

We find:

$$a^* \approx 24.3 \pm 0.5 \text{ Å} \qquad 5.2.5$$

The n=2 orbit will have a radius $\sim$100Å.

Comparing this result with Δr in eqn. 5.2.3, we see that the spatial extent of $\varphi(\vec{r}_1)$ is closest to the 1s hydrogenic state of the neutral donor. This might be expected from the large relative intensity of the $I_{2o} \rightarrow$1s transition. The fact that

$\Delta r > a^*$, however, indicates that there will be a mixing with the excited hydrogenic states 2s, 2p etc. This is in agreement with our observations of transitions from I_{2o} to the bound states of the neutral donor.

5.3 Attempts to Observe Weaker Two-Electron Lines

Transitions from I_{2o} to hydrogenic states of principal quantum number $n>3$ are difficult to observe with the intensity of light available from the monochromator. This led us to look for a laser source to pump the $I_{2o} \rightarrow 1s$ transition (4869.2Å). Triply ionized Xeon gas has a transition at 4869Å, but the corresponding laser line is too weak for our purposes. The only other discrete line in this wavelength region is the strong 4880Å transition of the Argon-ion laser. The problem was to bring the $I_{2o} \rightarrow 1s$ transition into resonance with the 4880Å line.

It is well-known that the band-gap reduces as temperature is increased. Since the weakly bound I_2 exciton complex essentially follows the band-gap, it is possible to bring the $I_{2o} \rightarrow 1s$ and 4880Å lines into resonance by raising the crystal temperature. This is clearly illustrated in Fig. 6. Resonance occurs at about 49°K. Fig. 7(a) is a spectrum of a crystal under 4880Å laser excitation, taken near the resonance temperature. The spectrum consists of one broad band and its LO

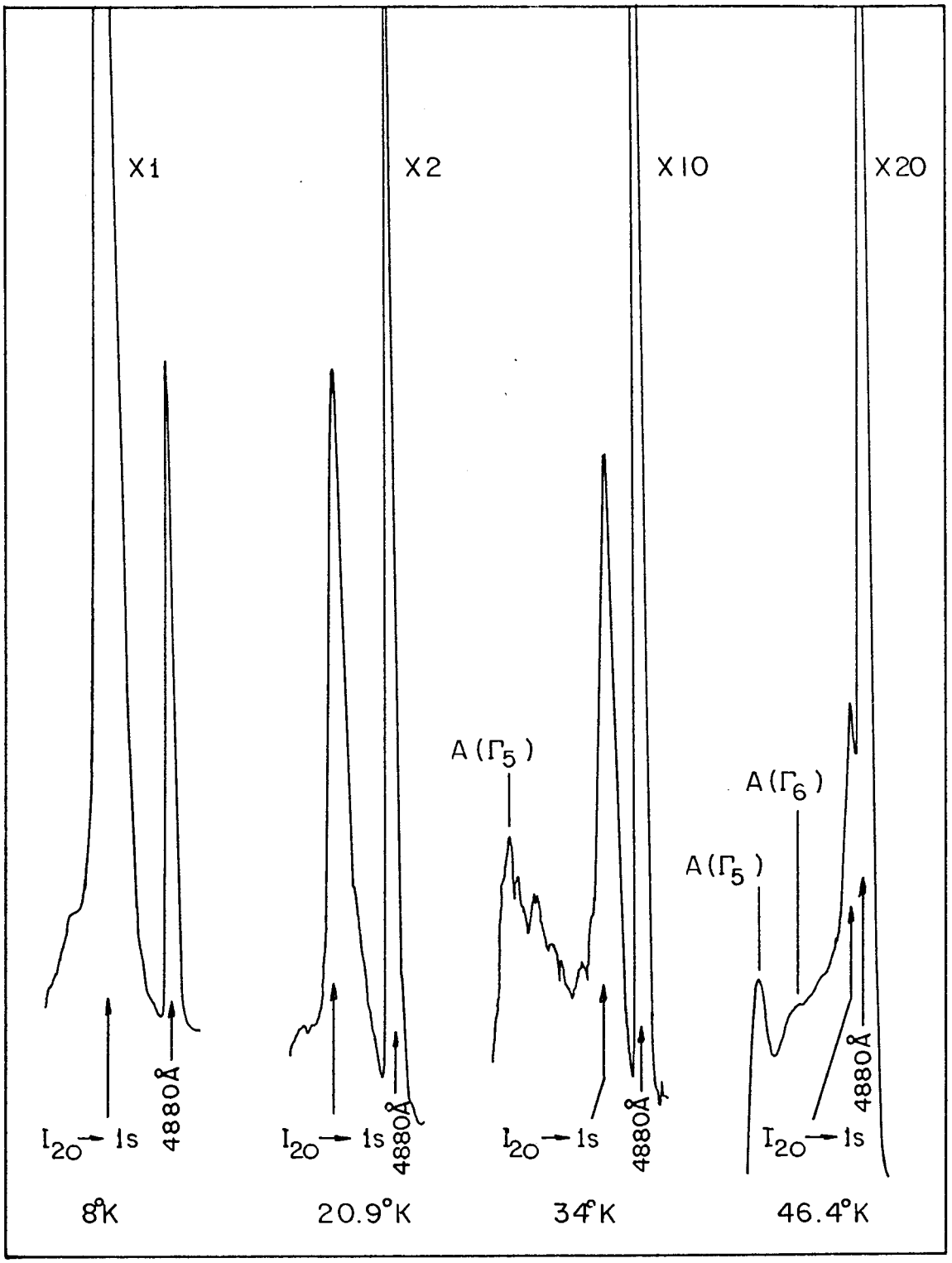

Fig. 6 An illustration of thermal tuning of the band-gap in CdS, in order to bring the $I_{2o} \rightarrow 1s$ and 4880Å transitions into resonance.

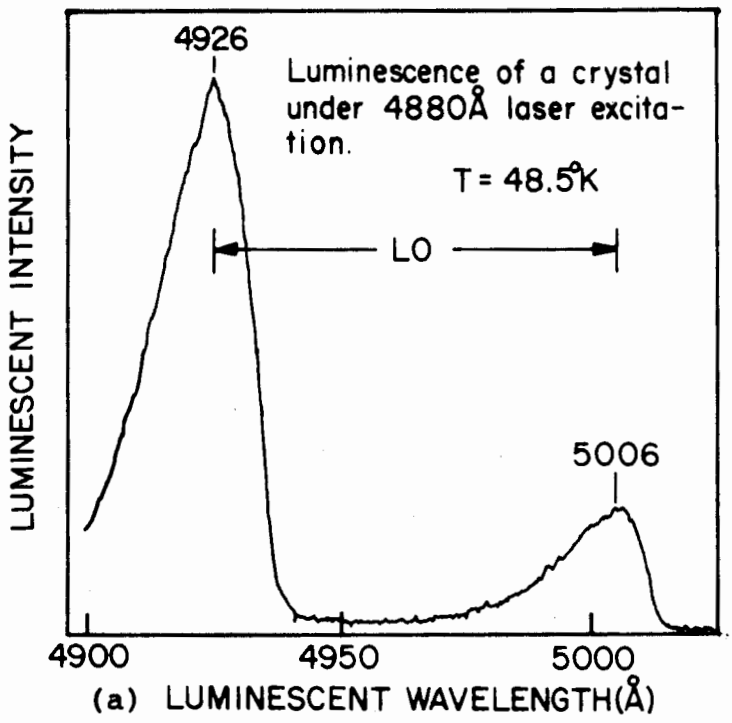

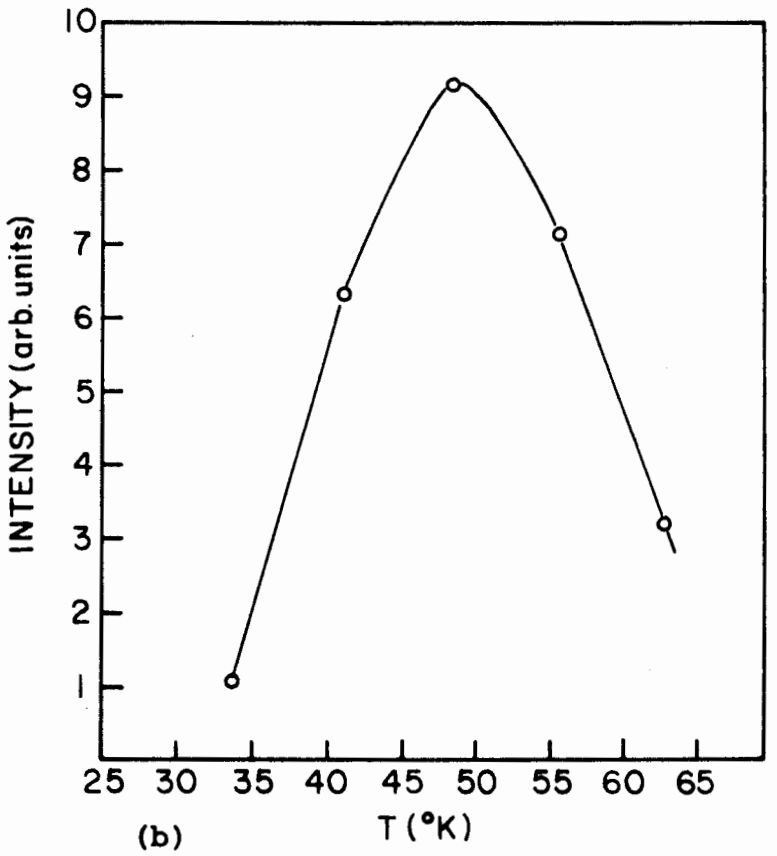

Fig. 7 (a) Luminescence under 4880Å excitation at 48.5°K.
(b) Temperature dependence of the luminescence.

replica. A plot of the peak intensity vs. temperature for this luminescent band is displayed in Fig. 7(b). As expected, the luminescent intensity is peaked at the resonance temperature.

The observed luminescence, although related to the I_2 complex as evidenced by Fig. 7(b), is not due to the two-electron transitions we wished to observe. We believe this emission band is due to the free exciton - bound exciton interaction discussed by Kukimoto, Shionoya and Kamejima (1971). This interaction proceeds as follows. An intrinsic A exciton scatters from an I_2 exciton complex and is dissociated into a free electron-hole pair; simultaneously the bound exciton decays radiatively, emitting a photon which is reduced in energy from the $I_{2o}\rightarrow 1s$ transition by the binding energy of the A exciton. At low temperatures, where we may neglect the kinetic energy of the A exciton, this results in a luminescent band peaked at 29.8mev, or the binding energy of the A exciton, below $I_{2o}\rightarrow 1s$.

Kukimoto et al (1971) were able to weakly observe this interaction at 1.8°K by intensely pumping the A exciton transition. At higher temperatures, however, the interaction should be more favored since the number of free and bound excitons becomes comparable due to thermal ionization of the I_2 complex (see Fig. 6). If we take the energy difference between the peak at 4926Å in Fig. 7(a) and the 4880Å

transition, and add to it a (3/2)KT term to account for the kinetic energy of the A exciton, we obtain 29.9±0.5 mev. This value agrees well with the A exciton binding energy, as required.

Since the exciton scattering interaction is favored at higher temperatures, and the resulting luminescence obliterates all features of the two-electron transitions, the thermal tuning technique cannot be used for our purposes. Another band-gap tuning technique, employed by Kukimoto et al.(1971), used the fact that doping CdS with Se to produce a mixed crystal system reduces the band-gap nearly in proportion to the selenium content. A mixed crystal $CdS_{1-x}Se_x$ with $x = 0.005$ was used to bring the A exciton transition at 1.8°K into resonance with the 4880Å line of the Argon-ion laser. From examination of their luminescent spectra, however, and our own experience with doped crystals, it is highly probable that the effects of the doping will wash out the finer features of the two-electron transitions.

Thus we must restrict ourselves to high purity crystals and low temperatures. It appears that the most likely source to perform the required experiment is a tuneable laser.

5.4 Summary and Conclusions

We have shown that the $I_{2o} \rightarrow 1s$ and two-electron transitions not only give information about the impurity center involved in a bound exciton complex, but also yield information about the nature of the bound exciton wavefunction. From the relative size of the discrete luminescent lines, corresponding to projection of the residual electron onto bound hydrogenic states, we concluded that the donor electron wavefunction in the presence of the exciton complex is strongly 1s-like. From considerations of the Radiative Auger band, it was found that the spatial extent of this wavefunction was somewhat larger than the corresponding 1s hydrogenic state. This larger size indicates the mixing with higher hydrogenic states which was evident from the discrete transitions.

It is apparent that higher excitation intensities are required in order to resolve the fine structure of the two-electron lines and to observe weaker transitions. Our experimental results demonstrate that thermal tuning to the 4880Å Argon-ion laser line is not a viable alternative. What is required is a tuneable laser source, such as a dye laser, which operates in the wavelength region of the I_2 transitions. The availability of such a source is dependent upon the existence of powerful lasers in the violet and u.v. wavelength regions. One possibility is a high frequency pulsed Nitrogen laser currently being developed.

PART II - LONG WAVELENGTH BOUND EXCITON EMISSION IN CdS

6. Long Wavelength Bound Exciton Emission - Theory

The theory is divided into three parts, each dealing with a separate process important in the interpretation of experimental data for the long wavelength exciton lines. Section 6.1 deals with absorption processes involving transitions between a band and a discrete level, and section 6.2 briefly discusses resonant exciton transfer between different impurities. The qualitative nature of these processes will prove useful in interpreting excitation spectra. The last section deals with the use of temperature quenching data to estimate binding energies for impurity centers.

6.1 Transitions From a Band to an Impurity Level

The theory of optical transitions between donor levels and the valence band, or between acceptors and the conduction band has been examined by W. P. Dumke (1963) and by E. J. Johnson (1968). Our ultimate interest lies in interpreting certain aspects of our excitation spectra in terms of a model allowing transitions from a band to a discrete level. In order to investigate the general behavior of the absorption coefficient for such a process, we shall consider the simple

case of transitions from the valence band to a shallow donor in a direct bandgap semiconductor.

The initial states, for a crystal of volume V, will have the form

$$\varphi_{n'k'}(\vec{r}) = \frac{1}{\sqrt{V}} e^{i\vec{k}'\cdot\vec{r}} U_{n'k'}(\vec{r}) \qquad 6.1.1$$

where $\varphi_{n'k'}(\vec{r})$ is the Bloch function of wave vector $\vec{k}'$ in valence band n'. Consider that the final state is the ground state $\Psi(\vec{r})$ of the donor impurity. $\Psi(\vec{r})$ may be expanded in terms of Bloch functions:

$$\Psi(\vec{r}) = \sum_{n,k} A_n(\vec{k})\varphi_{nk}(\vec{r}) \qquad 6.1.2$$

where the index n refers to the number of the band to which the Bloch function belongs. The absorption coefficient α will then be proportional to a sum of squares of optical matrix elements:

$$\alpha \sim \sum_{\substack{n',k' \\ n,k}} |\langle\Psi|e^{i\vec{q}\cdot\vec{r}}\vec{p}|n'k'\rangle|^2 \qquad 6.1.3$$

where $\vec{q}$ is the wave vector of the incident radiation and $\vec{p}$ is the electron momentum operator.

Since the screened coulomb force of the donor is assumed very weak, only the lowest order band will contribute sig-

nificantly to 6.1.2.

$$\Rightarrow \quad \Psi(\vec{r}) \approx \sum_k A_o(\vec{k})\varphi_{ok}(\vec{r})$$

$$= \frac{1}{\sqrt{V}} \sum_k A_o(\vec{k}) e^{i\vec{k}\cdot\vec{r}} U_{ok}(\vec{r}) \qquad 6.1.4$$

Also, since the conduction band minimum in CdS is at $\vec{k}=0$, $A_o(\vec{k})$ will be confined to the neighborhood of $\vec{k}=0$ and to lowest order we may write

$$U_{ok}(\vec{r}) \approx U_{oo}(\vec{r}) \qquad 6.1.5$$

Substituting into eqn. 6.1.4:

$$\Psi(\vec{r}) \sim \frac{1}{\sqrt{V}} U_{oo}(\vec{r}) \sum_k A_o(\vec{k}) e^{i\vec{k}\cdot\vec{r}}$$

$$= U_{oo}(\vec{r}) F(\vec{r}) \qquad 6.1.6$$

where

$$F(\vec{r}) = \frac{1}{\sqrt{V}} \sum_k A_o(\vec{k}) e^{i\vec{k}\cdot\vec{r}} \qquad 6.1.7$$

is the hydrogenic envelope function for the donor impurity (Kohn 1957). The normalized wave function for the ground state is given by

$$F(\vec{r}) = \frac{1}{(\pi a^{*3})^{\frac{1}{2}}} e^{-r/a^*} \qquad 6.1.8$$

a^* is the effective Bohr radius of the donor impurity. Invert-

ing eqn. 6.1.7 and using 6.1.8 we have:

$$A_o(\vec{k}) = \frac{1}{\sqrt{V}} \left(\frac{1}{\pi a^{*3}}\right)^{\frac{1}{2}} \int e^{-r/a^*} e^{-i\vec{k}\cdot\vec{r}}\, d^3\vec{r}$$

$$= \frac{8\pi^{\frac{1}{2}}}{V^{\frac{1}{2}} a^{*5/2}} \frac{1}{(k^2 + \frac{1}{a^{*2}})^2} \qquad 6.1.9$$

Using this result in 6.1.6:

$$\Psi(\vec{r}) \sim U_{oo}(\vec{r}) \frac{8\pi^{\frac{1}{2}}}{V^{\frac{1}{2}} a^{*5/2}} \sum_k \frac{e^{i\vec{k}\cdot\vec{r}}}{(k^2 + \frac{1}{a^{*2}})^2} \qquad 6.1.10$$

The matrix elements in 6.1.3 now become (omitting some constant factors)

$$M_{n'k'} \sim \frac{1}{a^{*5/2}} \int e^{-i\vec{k}'\cdot\vec{r}}\, U^*_{n'k'}(\vec{r})\, e^{i\vec{q}\cdot\vec{r}} \sum_k \frac{e^{i\vec{k}\cdot\vec{r}}}{(k^2+1/a^{*2})^2} U_{oo}(\vec{r})\, d^3\vec{r}$$

6.1.11

$$= \frac{1}{a^{*5/2}} \sum_k \frac{1}{(k^2+1/a^{*2})^2} \int e^{-i(\vec{k}'-\vec{k}-\vec{q})\cdot\vec{r}}\, U^*_{n'k'}(\vec{r})\, (\vec{p}+\hbar\vec{k})\, U_{oo}(\vec{r})\, d^3\vec{r}$$

$= 0$ unless $\vec{k}'-\vec{k}-\vec{q} = 0$

$\Rightarrow$ $\vec{k}' \approx \vec{k}$ since the wave vector of the incident light $\vec{q} \approx 0$.

$$\therefore\ M_{n'k'} \sim \frac{1}{a^{*5/2}(k^2+1/a^{*2})^2} \int U^*_{n'k}(\vec{r})\ (\vec{p}+\hbar\vec{k})\, U_{oo}(\vec{r})\, d^3\vec{r}$$

$$= \frac{1}{a^{*5/2}(k^2+1/a^{*2})^2} \int U^*_{n'k}(\vec{r})\ \vec{p}\ U_{oo}(\vec{r})\ d^3\vec{r}$$ from orthogonality of Bloch functions

$$\therefore\ M_{n'k} \sim \frac{P_{n'o}}{a^{*5/2}(k^2+1/a^{*2})^2}$$

where $P_{n'o}$ is the momentum matrix element for transitions from the n'^{th} valence band to the conduction band. Since the valence bands are rather far apart in CdS (see Fig. 1), we shall consider transitions only from the n'=0 or lowest order valence band. This eliminates the summation over n' in 6.1.3.

Thus the matrix elements are given by

$$M_{ok} \sim \frac{1}{a^{*\,5/2}\,(k^2+1/a^{*2})^2} \qquad \text{(aside from constant factors)} \qquad 6.1.12$$

Using 6.1.12 and changing the summation over k in eqn. 6.1.3 to an integration, we obtain

$$\alpha(\omega) \sim \frac{1}{a^{*5}} \int d^3\vec{k} \left(\frac{1}{k^2+1/a^{*2}}\right)^4 \delta(E-\hbar\omega+E_g-E_D) \qquad 6.1.13$$

The delta function ensures that the integration in 6.1.13 is restricted to those transitions satisfying the conservation of energy.

E_g = direct band gap; E_D = binding energy of donor.

Assuming the valence band is parabolic:

$$E = \frac{\hbar^2 k^2}{2m_h^*} \qquad 6.1.14$$

With eqn. 6.1.14 and the transformation $d^3\vec{k} = k^2 \sin\theta d\theta d\phi dk$,

eqn. 6.1.13 becomes:

$$\alpha(\omega) \sim \frac{1}{a^{*5}} \int \frac{dE\ \sqrt{E}}{\left(\frac{2m_h^* E}{\hbar^2} + \frac{1}{a^{*2}}\right)^4} \delta(E-\hbar\omega+E_g-E_D)$$

$$= \frac{a^{*3}(\hbar\omega-E_g+E_D)^{\frac{1}{2}}}{\left(\frac{2m_h{}^* a^{*2}(\hbar\omega-Eg+E_D}{\hbar^2} + 1\right)^4} \qquad 6.1.15$$

Using $m_e^* = \hbar^2/(2a^{*2}E_D)$, where m_e^* is the electron effective mass, the above expression becomes

$$\alpha(\omega) \sim \frac{a^{*3}(\hbar\omega-E_g+E_D)^{\frac{1}{2}}}{\left(\frac{m_h^*}{m_e^*}\ \frac{1}{E_D}\ (\hbar\omega-E_g+E_D)\ +1\right)^4} \qquad 6.1.16$$

Aside from some constant factors, eqn. 6.1.16 is the absorption coefficient for transitions from the valence band to the ground state of a shallow donor. A more complete expression may be found in Dumke (1963). $\alpha(\hbar\omega)$ is plotted in Fig. 8. As would be expected, there is no absorption for $\hbar\omega < (E_g - E_D)$. Allowing transitions to excited states of the impurity will broaden $\alpha(\hbar\omega)$ but the high energy cut-off at $(E_g - E_D)$ will be unchanged. The behavior of the absorption coefficient for any process involving transitions from a band to a discrete level will be qualitatively the same as $\alpha(\hbar\omega)$ in Fig. 8.

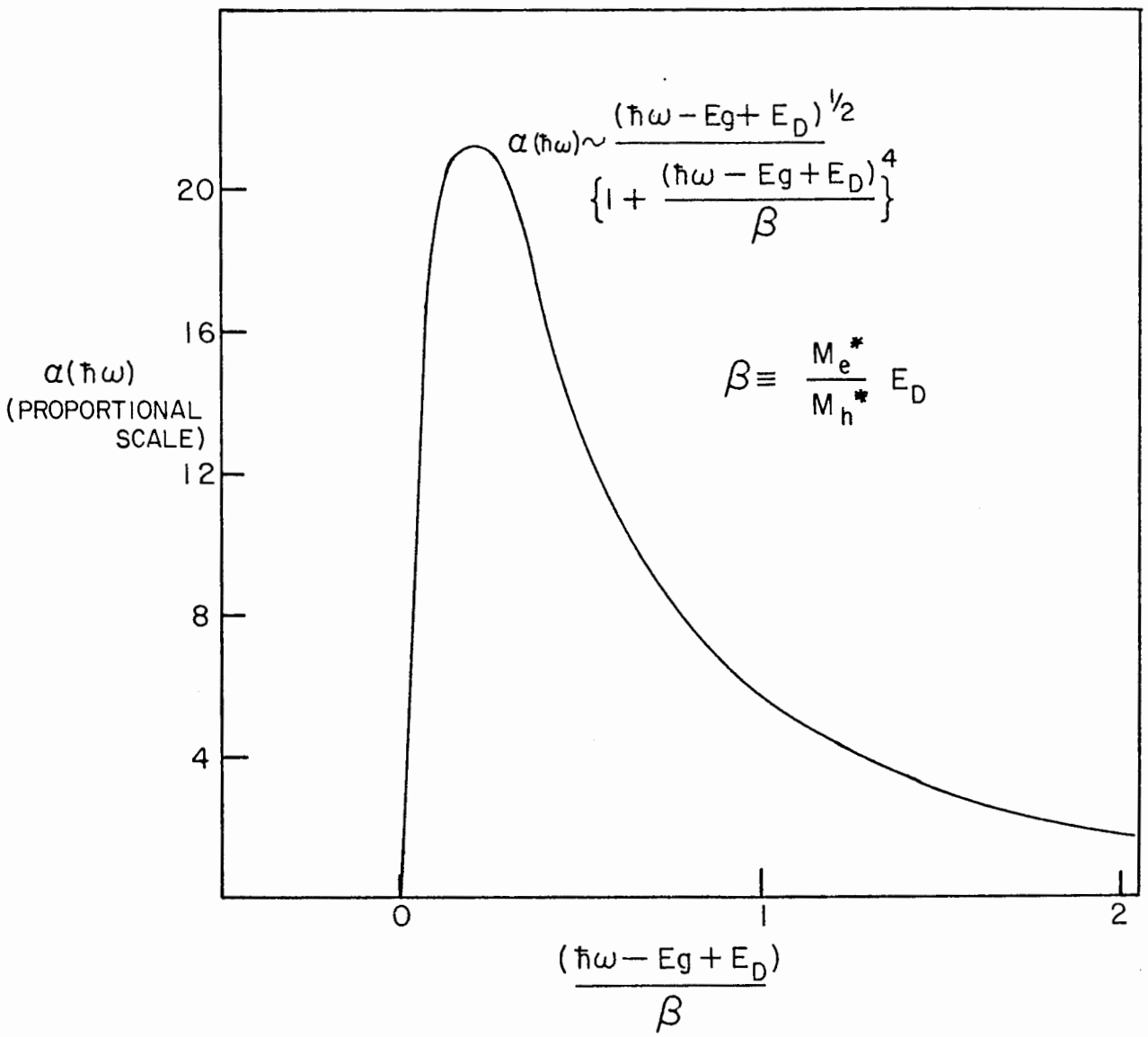

Fig. 8 A plot of $\alpha(\hbar\omega)$ for transitions between the valence band and a shallow donor.

6.2 Resonant Energy Transfer

The current theory of transfer of electronic energy by the resonance interaction between an excitation localized on one impurity and an unexcited state at another is due primarily to T. Forster and D. L. Dexter. Reviews may be found in Dexter (1953) and Dexter and Knox (1965). The particular case of the initial and final states being bound excitons on two chemically different impurities in a solid has been treated by Dow (1968). The initially excited impurity is called the sensitizer S and the initially unexcited impurity is called the activator A. The perturbation inducing the resonant exciton transfer is the sum of all coulombic interactions of the outer electrons, holes and core of A with those of S, reduced by the dielectric constant κ of the medium. The perturbation Hamiltonian then has the form of a double sum over all particles of S and A:

$$H' = \sum_{i<} \sum_{j} \frac{e_i e_j}{\kappa |\vec{r}_i - \vec{r}_j|} \qquad 6.2.1$$

Eqn. 6.2.1 may be expanded in a multipole series which, in the simplest approximation, is limited to the dipole-dipole term (see Dexter 1953):

$$H' \approx \frac{e^2}{\kappa R^3} \{\vec{M}_S \cdot \vec{M}_A - 3(\vec{M}_S \cdot \frac{\vec{R}}{R})(\vec{M}_A \cdot \frac{\vec{R}}{R})\} \qquad 6.2.2$$

R = internuclear separation of S and A

$\vec{M}_{A/B}$ = dipole moment of activator/sensitizer

H' in eqn. 6.2.2 is the same interaction which gives rise to Van der Waals' forces. In a system which is dilute, so that the wavefunction overlap between sensitizer and activator may be neglected, the dipole-dipole term will be the dominant contribution to H', provided the sensitizer has an allowed radiative transition.

Proceeding by means of first order time-dependent perturbation theory (a complete derivation may be found in Dexter 1953), the average dipole-dipole resonance transition rate P may be expressed in the form

$$P = \frac{1}{\tau_S} \frac{R_o^6}{R^6} \qquad 6.2.3$$

where $$R_o^6 = \frac{3\hbar^4 c^4 Q_A}{4\pi n^4} \int \frac{F_S(E) F_A(E)}{E^4} dE \qquad 6.2.4$$

is the critical transfer distance at which spontaneous emission and resonance transfer to A are equally probable decay channels for S.

n = refractive index of the medium

τ_S = radiative lifetime of the sensitizer

Q_A is the area under the activator absorption spectrum

$$\equiv \int \frac{\alpha_A(E)}{N_A}\, dE \qquad \text{where } \alpha_A = \text{absorption coeff. for activator}$$

$$N_A = \text{no. of activator centers}$$

$F_A(E)$ is the activator absorption normalized to unity

$F_S(E)$ is the normalized sensitizer emission.

Thus the integral in 6.2.4 is essentially the energy overlap between the activator absorption and sensitizer emission spectra.

In the event that the wavefunction overlap between the sensitizer and activator is not negligible, there will be an additional term in eqn. 6.2.2 due to an exchange interaction (Dexter 1953). In some physical situations, this may be comparable to the dipole-dipole interaction.

6.3 Dependence of Luminescent Efficiency on Temperature

In many cases, the thermal quenching of luminescence can be explained in terms of a nonradiative decay, proceeding via a thermal activation process, which competes with radiative decay. The probability of nonradiative decay will have the form

$$\frac{1}{\tau(T)} = \frac{1}{\tau_o}\, e^{-E_a/KT} \qquad 6.3.1$$

where $1/\tau_o$ is a frequency factor and E_a is the activation

energy for the process. If we assume the radiative decay probability $1/\tau_R$ is temperature independent, then the quantum efficiency $\eta(T)$ of the luminescence (the ratio of emitted quanta to total absorbed quanta in the steady state) is:

$$\eta(T) = \frac{1}{1 + \frac{\tau_R}{\tau_o} e^{-E_a/KT}} = \frac{1}{1 + \beta e^{-E_a/KT}} \qquad 6.3.2$$

where β is a constant. Since nonradiative processes have much shorter lifetimes than radiative transitions, $\beta >> 1$.

In terms of intensity of the luminescence, eqn. 6.3.2 may be written

$$I(T) = \frac{I_o}{1+\beta e^{-E_a/KT}} \qquad 6.3.3$$

where I_o is the intensity at $T = 0$. If the intensity $I(T)$ is known at low temperatures, an estimate of I_o may be obtained by extrapolation. Then $\ell n(I_o/I(T) - 1)$ may be plotted vs. $1/T$ to give a straight line whose (negative) slope yields the activation energy E_a. Such a procedure has been used by Yakobson (1964) to measure the binding energies of the A exciton in the I_1 and I_2 complexes in CdS. The values obtained were in very good agreement with those calculated from luminescent spectra.

Even in cases where a reasonable estimate of I_o cannot be made, the activation energy may be found in the temperature

region where $\exp(-E_a/KT) >> 1$. Then:

$$I(T) \simeq \beta' e^{E_a/KT} \qquad 6.3.4$$

Thus a plot of $\ell n(I(T))$ vs. $1/T$ should be linear at sufficiently high temperatures, with slope proportional to E_a. This technique has been used by Maeda (1965) to find the activation energy of the bound-to-bound emission in CdS.

7. Long Wavelength Bound Exciton Emission - Experimental Results and Discussion.

Our investigations have uncovered a family of some 8 narrow, long wavelength lines, including the I_6 and I_7 transitions reported by Reynolds and Litton (1963). These lines are illustrated in Fig. 9, a spectrum taken in mode (i), and are listed in Table V. Although many samples were studied from different lots of ultra-high purity and compensated crystals, the line reported by Reynolds and Litton (1963) at 5068 Å (see Table II) was not observed. There is, however, a strong 5065Å line which has been labeled I_{6a} in keeping with their notation.

Polarization measurements for $E \perp c$ and $E \parallel c$ were made by inserting a polaroid element between the crystal and the analyzing spectrometer. Care was taken to account for the polarization effects of the spectrometer, either by calibration with an unpolarized source or by use of a depolarizing element. The polarization of all long wavelength lines was generally quite weak and varied from sample to sample. The results in Table V are from a concensus of polarization measurements on several crystals. The polarization for I_7 in Table V does not agree with the result quoted by Reynolds and Litton (1963) in Table II. This discrepancy is probably due to the sample dependence of the polarization.

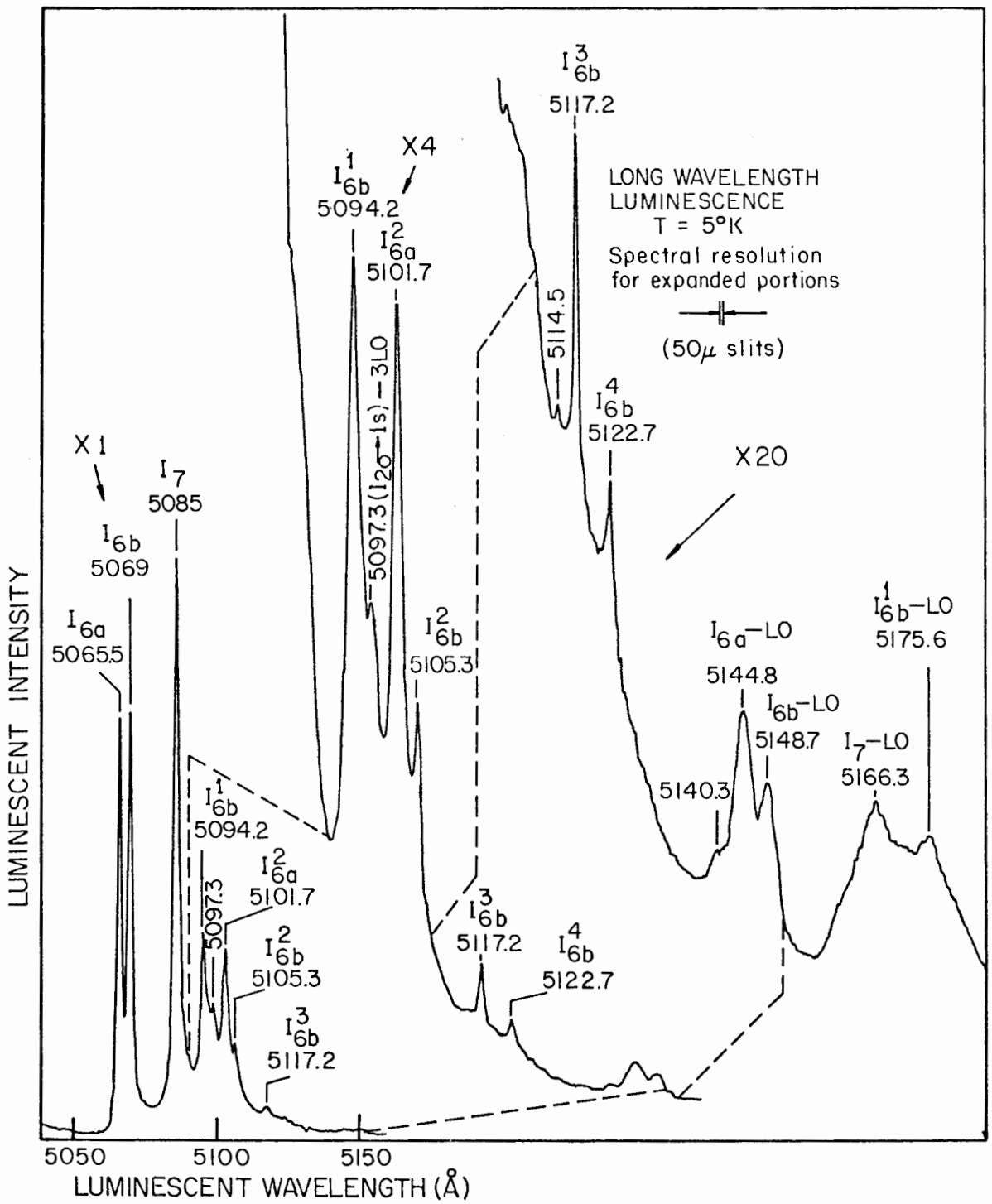

Fig. 9 Luminescent spectrum at 5°K showing long wavelength exciton emission. The crystal was from lot #356.

Table V Long Wavelength Exciton Lines in CdS

Line	Position λ(Å)	E(ev)	E_g-E(mev)	Polarization
I_{6a}	5065.5	2.44694	136.1	E⊥c
I_{6b}	5069	2.44525	137.8	E||c
	[1]5079.6	2.44015	142.8	
I_7	5085	2.43756	145.4	E⊥c
I^1_{6b}	5094.2	2.43316	150	E||c
	[2]5097.3	2.43168	151.3	
I^2_{6a}	5101.7	2.42958	153.4	unpolarized
I^2_{6b}	5105.3	2.42787	155.1	unpolarized
	[1]5114.5	2.42350	159.5	
I^3_{6b}	5117.2	2.42222	160.8	
I^4_{6b}	5122.7	2.41962	163.4	

[1] very weak lines; The line at 5079.6Å may be seen in Fig.2.

[2] probably (I_{2o}→1s)-3LO from energy considerations

The lines in Table V which have the same subscript a (or b) are believed to be transitions from the same state of the I_6 complex to different final states of the impurity center. This is somewhat analogous to the two-electron transitions discussed in connection with the I_2 complex. Investigation of the long wavelength lines was carried out by means of excitation spectra (mode (iii)) of the stronger lines, variation of the sample temperature and intensity of the exciting light, and infrared irradiation. Each of these experiments will be discussed in a separate section.

7.1 Results of Excitation Spectra

7.1.1 The I_2 Complex

A knowledge of the behavior of the I_2 complex is of some importance to the discussions in this section. The excitation spectra of the $I_{2o} \rightarrow 1s$ (4869 Å) and $I_{2o} \rightarrow n = 2$ (4916 Å) transitions are displayed in Fig. 10 (a) and (b). It is interesting to note that the resonances at the free exciton transitions are very weak. Only small peaks appear at the A (n = 1) Γ_5 and Γ_6 lines and the resonance at A(n = 2) is almost nonexistant. There is apparently no resonance at all for the B exciton.

This indicates that free excitons, for the most part, are not being captured to form bound complexes. The

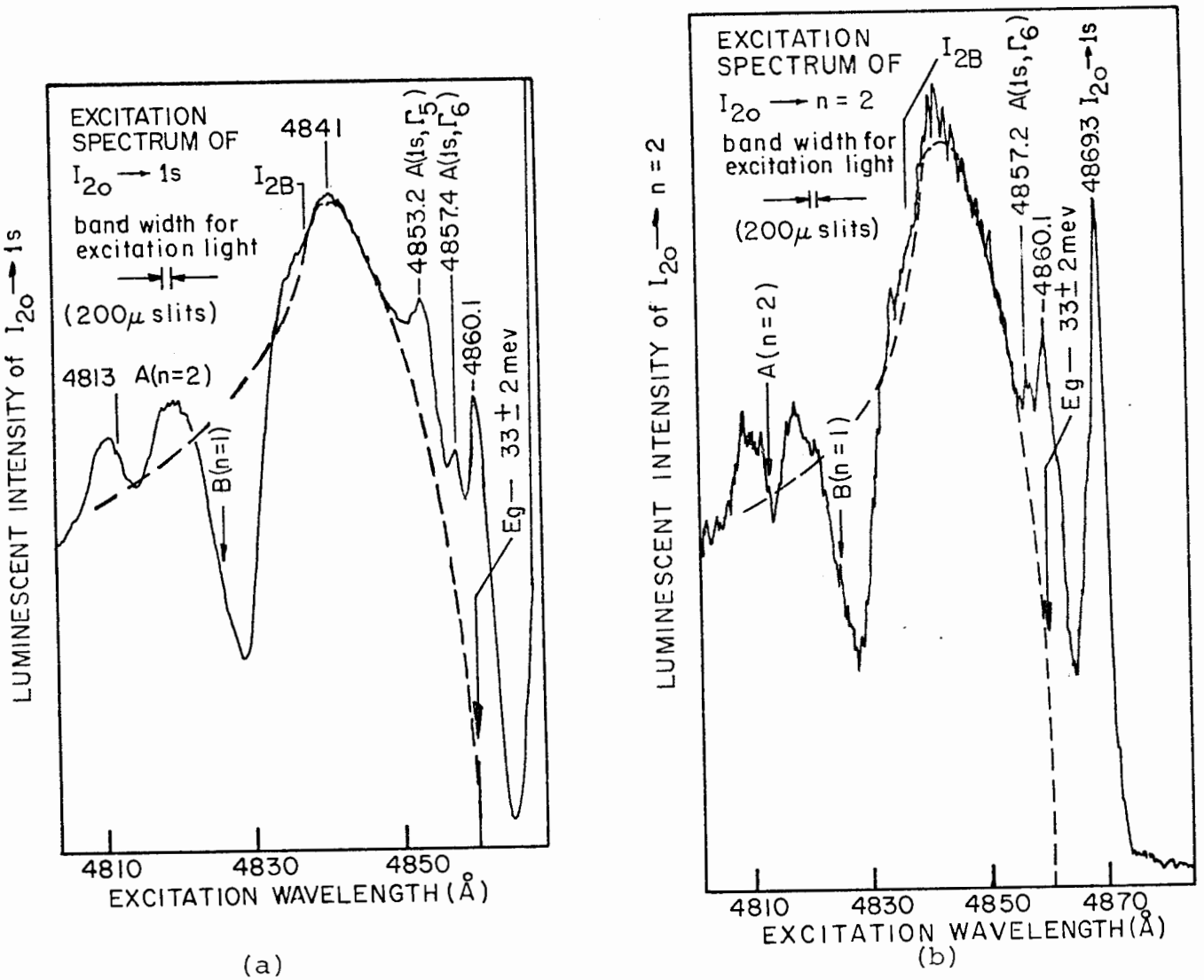

Fig. 10 (a) Excitation spectrum of the $I_{2o} \rightarrow 1s$ transition. (b) Excitation spectrum of the $I_{2o} \rightarrow n=2$ transition, which includes both the $I_{2o} \rightarrow 2s$ and $I_{2o} \rightarrow 2p_x$, $2p_y$ lines mentioned in section 5.1.

excitons may be recombining via surface states, or, if the sample is very pure, the time required for the exciton to migrate to a Cl site may be longer than its decay lifetime. This means that the bound excitons in our samples are created directly or by sequential capture of an electron and hole, rather than by free exciton capture.

The lack of resonance at the intrinsic exciton transitions gives the excitation spectra a 1-R appearance, where R is the reflection coefficient. Thus the dips near the free exciton lines are due to resonances in the reflection spectra. In agreement with the results of Thomas and Hopfield (1959), the resonant frequencies of the exciton transitions lie at about 1 mev higher photon energies than the corresponding reflection dips.

The peak at 4860 Å in Fig. 10 (a) and (b) is due to an excited state of the I_2 complex (Malm and Haering 1971a). The line at 4869 Å in Fig. 10 (b) is the familiar $I_{2o} \rightarrow$ 1s transition.

There is a large band to the high energy side of the excitation spectra in Fig. 10. This band begins at about 4860 Å, is peaked at 4841 Å, and extends to shorter wavelengths. If the crystal is illuminated with light of wavelength near 4841 Å (mode (ii)), it is found that all luminescent transitions at longer wavelengths are excited. This indicates that free carriers are being created even

though the exciting light is below band-gap, and not near any known resonant absorption line.

The general appearance of the band in Fig. 10 is similar to that of the absorption coefficient discussed in section 6.1, in connection with transitions from the valence band to a discrete level. The low energy cut-off of the excitation band in Fig. 10 is 33 ± 2 mev, or approximately the Cl donor binding energy, below the band-gap. With reference to section 6.1, this might imply that there are ionized donors in the sample which are being filled by exciting electrons from the valence band. Although such a process creates neutral donors and free holes, it is difficult to see why it should give rise to the resonance in Fig. 10. In particular, compensated crystals, which have a large number of ionized donors, show no such structure (see Malm 1971). It is possible to imagine a resonance mechanism, however, if we allow the existence of shallow hole traps of approximately the same binding energy as the Cl donor. Then excitation in the region of 4841Å would provide electrons for the ionized donors and holes for the hole traps, in the manner described in section 6.1. This would not only enhance the number of neutral donors, but would create free electrons and holes. Such a mechanism might explain the observed excitation band and the fact that all luminescent lines of the crystal are excited by light in this wavelength region. The shallow hole

traps suggested here may be provided by the center giving rise to the I_6 complex, as will be indicated in section 7.1.2.

7.1.2 The I_6 Complex

The intensity of the long wavelength lines relative to the $I_{2o} \rightarrow 1s$ transition was found to be very sample dependent. In samples where this relative intensity was small, excitation spectra with reasonable resolution could be obtained for only I_{6b} and I_7, since all other lines were too weak at the excitation intensities provided by the monochromator (dependence on excitation intensity is discussed in section 7.3). A typical excitation spectrum of I_{6b} (5069Å) from such a sample is shown in Fig. 11. In addition to some relatively sharp lines, the spectrum consists of two broad bands which have been labelled A and B. The first, band A, begins at about 4880Å, is peaked at about 4850Å and extends to higher energies. The spectrum in this region has a 1-R appearance, with dips corresponding to the $A(n=1,\Gamma_5)$, $B(n=1)$ and $A(n=2)$ free excitons, indicating that the I_6 complex has a very small free exciton capture cross-section. The sketch of A in Fig. 11 has been made to compensate for the reflection dips. Band B is essentially a continuum which begins at about 5000Å and merges with band A at higher energies. The low energy cut-offs for bands A and B are 43 ± 3 mev and 104 ± 2 mev below the band-gap, as indicated in Fig. 11.

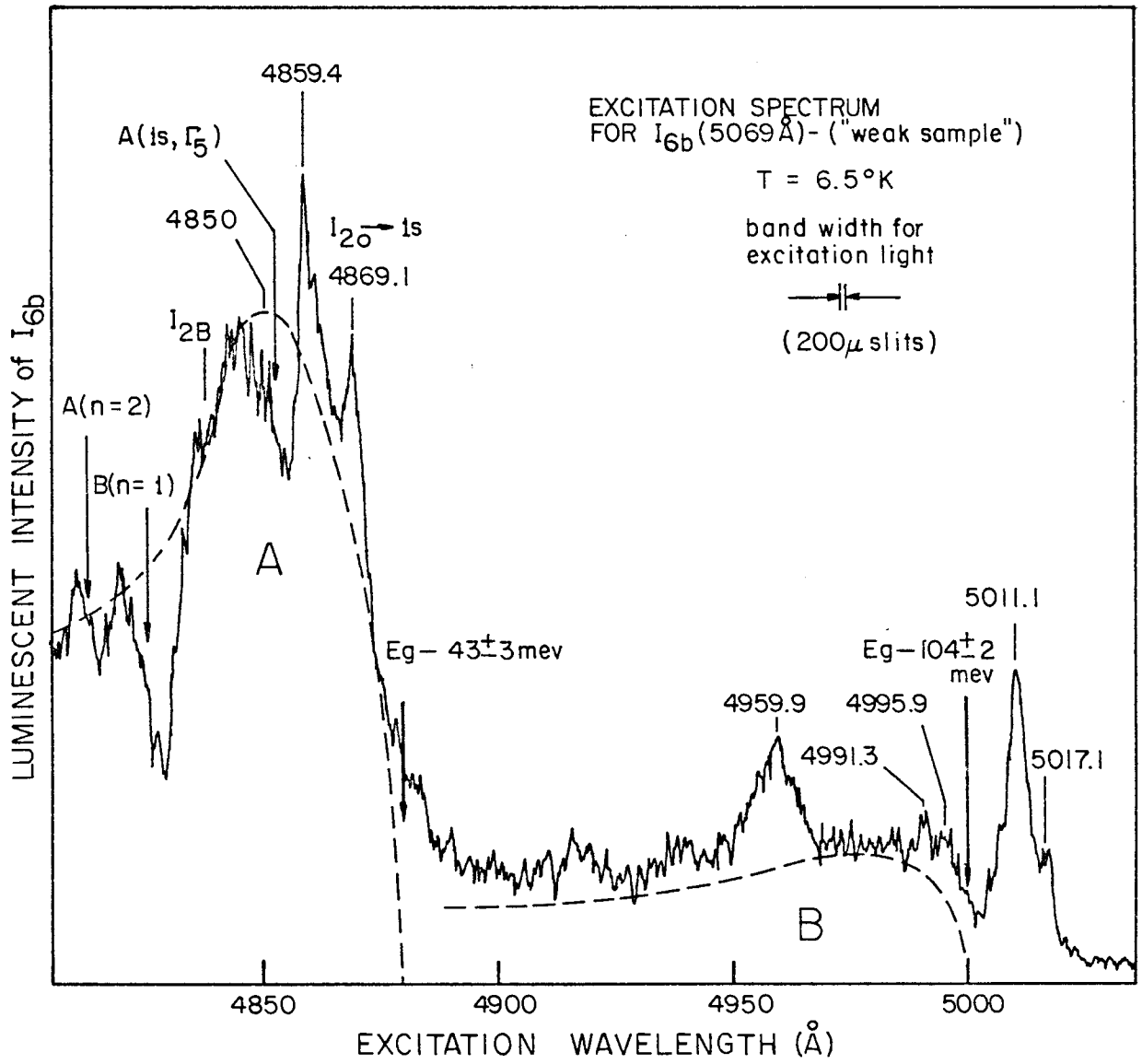

Fig. 11 Excitation spectrum of I_{6b} from a sample where the long wavelength lines were weak relative to the I_{2o}→1s transition.

One possible interpretation of A and B may be made in terms of a model allowing transitions from a band to bound states provided by the I_6 complex. This interpretation is facilitated if we assume that the impurity center giving rise to I_6 is capable of binding an electron by about 104 mev and a hole by about 43 mev, corresponding to the long wavelength edges of band B and band A, respectively. The more shallow state is assigned to the hole in order to explain the resonance band in Fig. 10, according to the qualitative analysis in section 7.1.1. Separating the electron and hole in the above manner can only be an approximation, since it ignores any correlation between the two. It is interesting to note, however, that this division of the total binding energy into two parts, corresponding to the binding of the individual electron and hole, has been used to describe an exciton bound to a Bi isoelectronic trap in GaP (Faulkner and Dean 1970), where the electron and hole binding energies are 69 mev and 38 mev, respectively. For our case, the binding energies measured from Fig. 11 predict (ignoring correlation) that the observed emission line should be about 147 ± 5 mev below the band-gap. This is in fair agreement with the value of 137.8 mev for I_{6b} in Table V.

From the above considerations, band B then corresponds to pumping an electron from the valence band to fill the bound state provided by our deep impurity. An excitation resonance

occurs since the exciton may be completed by capture of the free hole left in the valence band, or by capturing a hole provided by some other nonresonant process. In a similar manner, band A corresponds to creation of a hole in the shallow hole state provided by the impurity center. The complex is then completed by subsequent capture of an electron.

In samples where the long wavelength lines are weak, relative to the $I_{2o} \rightarrow 1s$ transition, the number of centers giving rise to I_6 is probably much smaller than the number of Cl donors. The impurity electron states will then be completely filled, at the expense of the Cl donors, since they are deeper than the donor binding energy. This explains why only a small resonance is seen for band B in Fig. 11 - all the electron states are already filled. This also explains the large relative intensity of band A for such samples - the exciton complex is directly created by providing a hole, since all the electron states are already filled. Also, this situation allows for the existence of ionized donors, as required by the qualitative model for the excitation band in Fig. 10, even for a case where there are essentially no acceptors. In samples where the number of I_6 impurity centers is greater than the number of donors, band B should be larger relative to band A, since there would then be empty electron impurity states.

The lines at 4869.1Å and 4859.4Å in Fig. 11 correspond to transitions from the ground and an excited state, respective-

ly, of the I_2 complex (Malm and Haering 1971a). There is also an indication of a resonance at the I_{2B} transition (4837.7Å). This implies that, while I_6 is not excited at the free exciton transitions, it can be excited by the bound I_2 exciton complex (see also Fig. 5). This excitation may take the form of a resonant exciton transfer (Dow 1968) from I_2 to the more deeply bound state represented by I_6. The fact that the 4859.4Å line is stronger than the 4869.1Å line in Fig. 11, in contrast to what is observed in excitation spectra of transitions from the I_2 complex in Fig. 10, indicates that the resonant transfer favors I_2 states having larger spatial extent. Such a process has the behavior more of an exchange interaction (Dexter 1953) than the dipole-dipole interaction briefly discussed in section 6.2. A qualitative understanding of the nature of any exciton transfer mechanism, however, requires more information about the nature of the impurity center giving rise to I_6.

Figs. 12, 13 and 14 are excitation spectra of I_{6a} (5065.5Å), I_{6b}(5069Å) and I^1_{6b}(5094.2Å), respectively, taken from the sample which showed the strongest long wavelength lines. The I_6 and I_7 transitions in this sample were almost as intense as the $I_{2o}\rightarrow 1s$ transition. This implies that the number of impurity centers giving rise to I_6 is probably of the same order as, or greater than, the number of donors. As has been predicted for such a sample, excitation band B is larger,

relative to band A, than in Fig. 11.

The similarity of the three spectra in Figs. 12, 13 and 14 is quite apparent. As before, resonances occur at the I_{2B} bound exciton and at about 4859.4Å and 4869.2Å, indicating the presence of a resonant exciton transfer process. It is interesting to note, in defense of the transfer process, that the $I_{2o} \rightarrow 1s$ transition is about an order of magnitude weaker for the sample in Fig. 13 than for the sample in Fig. 11. Also, the ratio of R_o^6 (eqn. 6.2.4) estimated from Fig. 13 to that estimated from Fig.11 is of the order of 10, implying that the transfer process is more probable for the sample in Fig. 13. Such arguments are very qualitative, however, and more work is required in this area.

No physical interpretation has been found for the peaks between 4871Å and 4960Å. From the size of the thermal activation energy for the I_6 complex (section 7.2), it is doubtful that any of these resonances correspond to excited states of I_6. Since an excitation spectrum $E(h\nu)$ is the product of the absorption spectrum $A(h\nu)$ and the probability $P(h\nu)$ that the photo-excited state decays to the observed luminescent line (Malm and Haering 1971b), these peaks may be due to resonances in $P(h\nu)$ rather than $A(h\nu)$. The peak at 4960Å has probably been exaggerated since it lies close to a strong line of the Hg arc lamp (see Fig. 3).

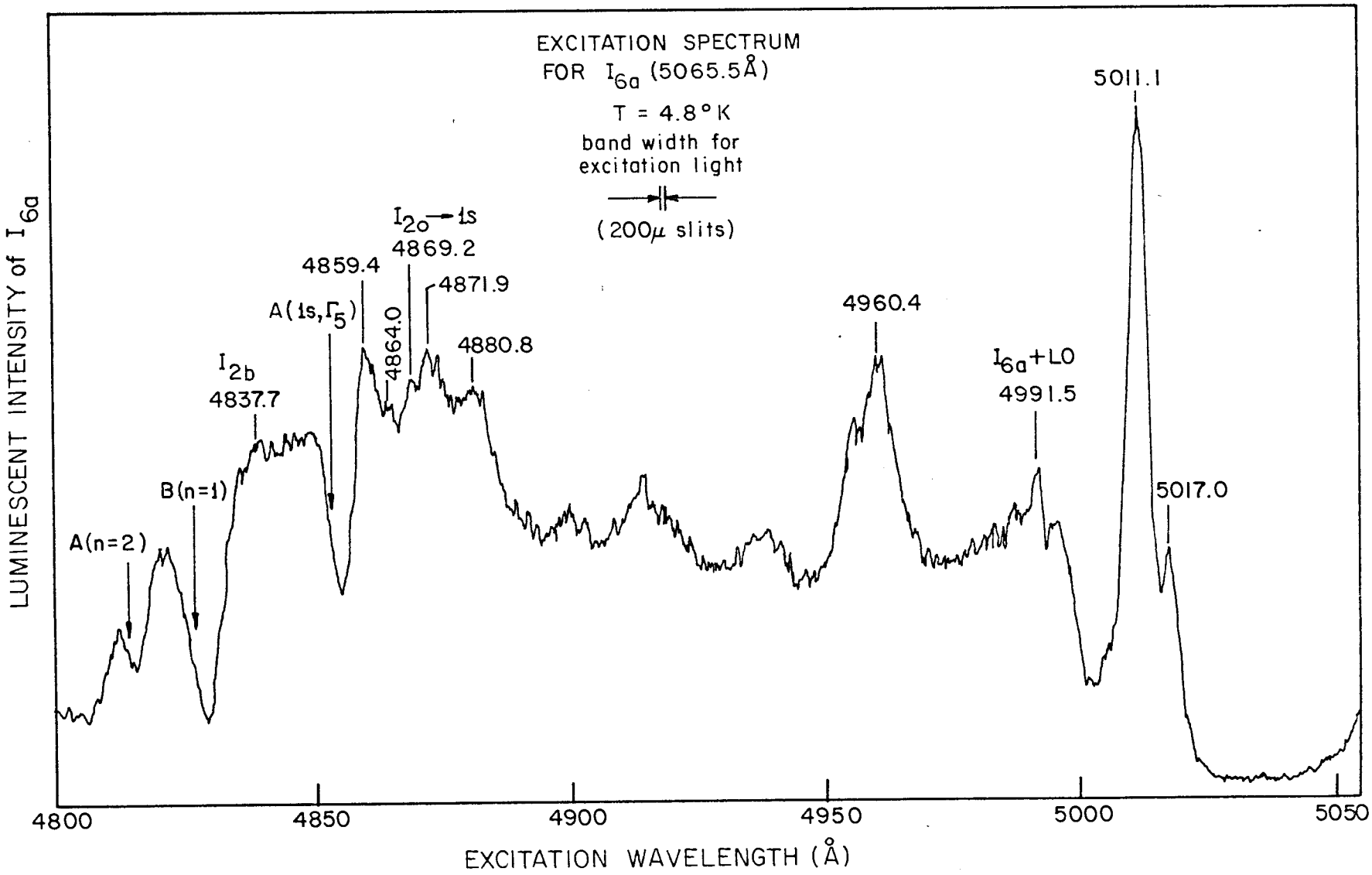

Fig. 12 Excitation spectrum of I_{6a} transition from a sample which displayed very strong long wavelength lines.

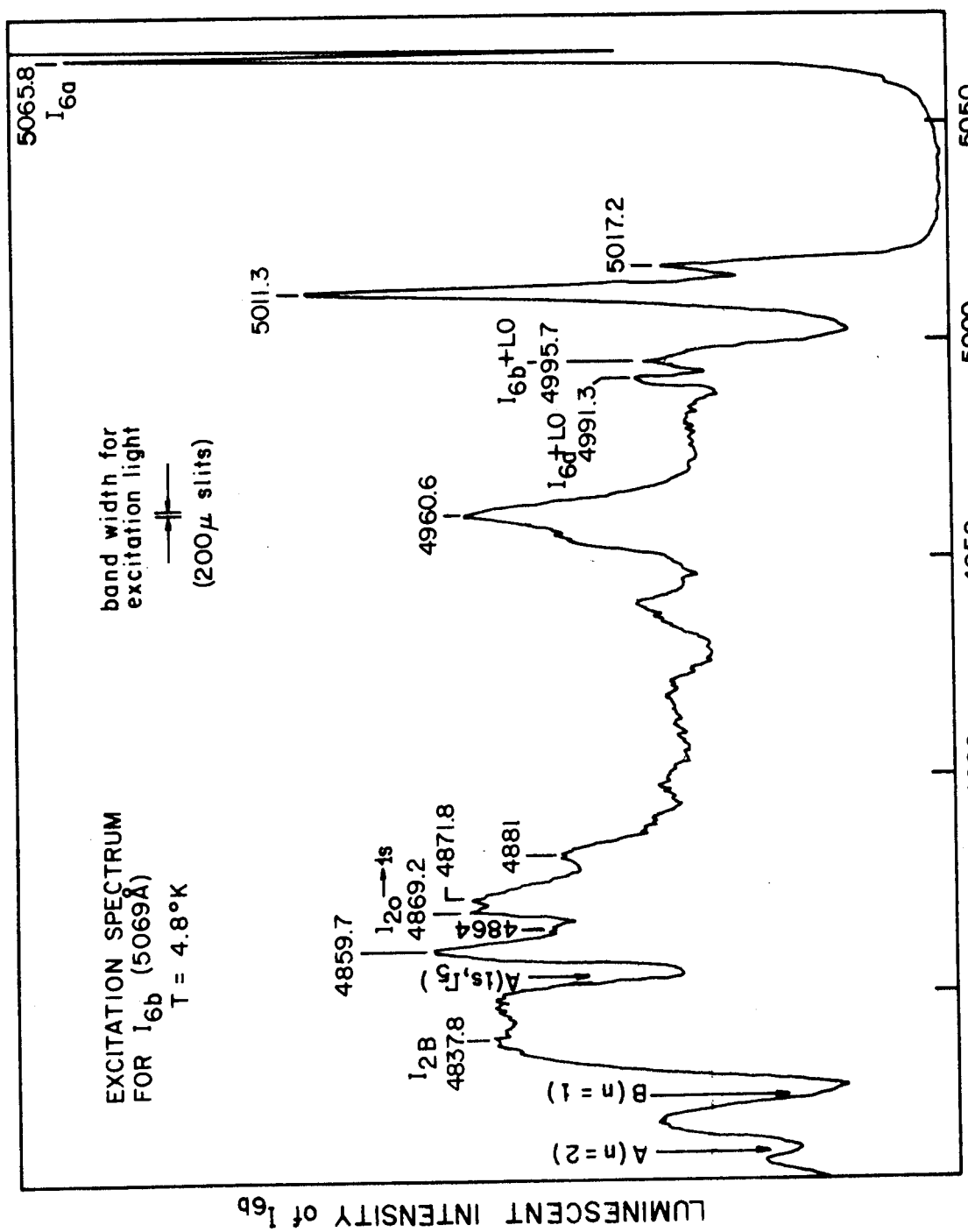

Fig. 13 Excitation spectrum for I_{6b} from a sample showing strong long wavelength lines.

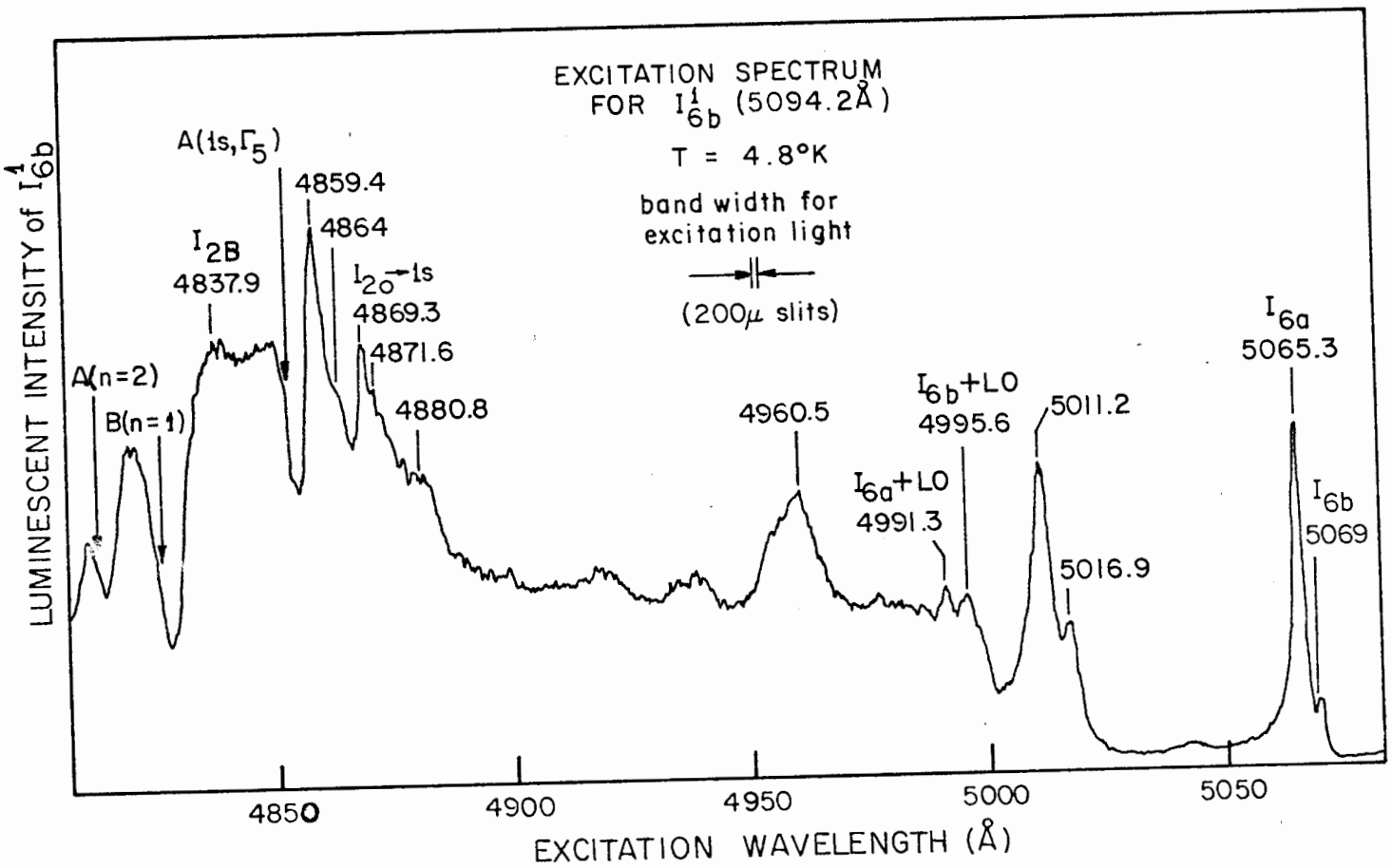

Fig. 14 Excitation spectrum of the I^1_{6b} transition from a sample which displayed very strong long wavelength lines.

One of the most revealing features of the excitation spectra of the I_6 lines (Figs. 12-14) is the presence of sharp resonances at the wavelengths corresponding to the I_{6a} and I_{6b} transitions. For example, the line at 5065.8Å in Fig. 13 indicates that I_{6b} may be excited by I_{6a}. From Fig. 14 we see that I_{6b}^1 may be excited by both I_{6a} and I_{6b}, with the former being more efficient, since the ratio $I_{6a}/I_{6b} \sim 10$. These results demonstrate an intimate relationship between all three lines. As will be indicated later, we believe that I_{6b} and I_{6b}^1 are transitions from the ground state of the I_6 complex, while I_{6a} is a transition from an excited state.

The peaks at 4991.3Å and 4995.7Å in Fig. 13 are one LO phonon energy above I_{6a} and I_{6b}, respectively. The phonon replica assignment is supported by the fact that the 4995.7Å line is missing in Fig. 12, the excitation spectrum of I_{6a}. This is consistent with the assumption that I_{6a} is an excited state of the I_6 complex. The sharp resonances at about 5011Å and 5017Å are most probably excited states of the I_6 complex (28mev and 25.2mev above I_{6b}, respectively). The fact that these lines have widths considerably larger than I_{6a} or I_{6b} (see Figs. 13 and 14), indicates rapid nonradiative relaxation to lower energies.

7.1.3 The I_7 Complex

Fig. 15 shows the excitation spectrum for I_7 (5085Å). The spectrum is remarkable for its simplicity - it consists primarily of a broad band at much higher energies than the actual radiative transition. This band has some similarities with band A in the excitation spectra of the I_6 lines. Both contain a broad peak at the I_{2B} transition and have a 1-R appearance. In Fig. 15 reflection dips appear corresponding to the A(n=1,Γ_6), A(n=1,Γ_5), A(n=2) and B(n=1) free excitons. There are, however, no excitation resonances in common with excited states of the I_2 complex. The fact that there is only one band in Fig. 15, as opposed to two in the excitation spectra of the I_6 lines, may indicate that I_7 is produced by the capture of only one particle (electron or hole) to produce a bound exciton complex. For example, a deep donor need only bind a hole to produce a complex analogous to I_3 (see section 2.2) but with a much higher binding energy.

The intensity of I_7 relative to the I_{6a} and I_{6b} transitions varies markedly from one group of samples to another, being very strong in some cases, such as Fig. 2, and almost zero in others. From this evidence and the excitation spectra of the long wavelength lines, it appears that I_6 and I_7 are two distinct complexes. There is, however, a weak coupling between the two as evidenced by the small resonances

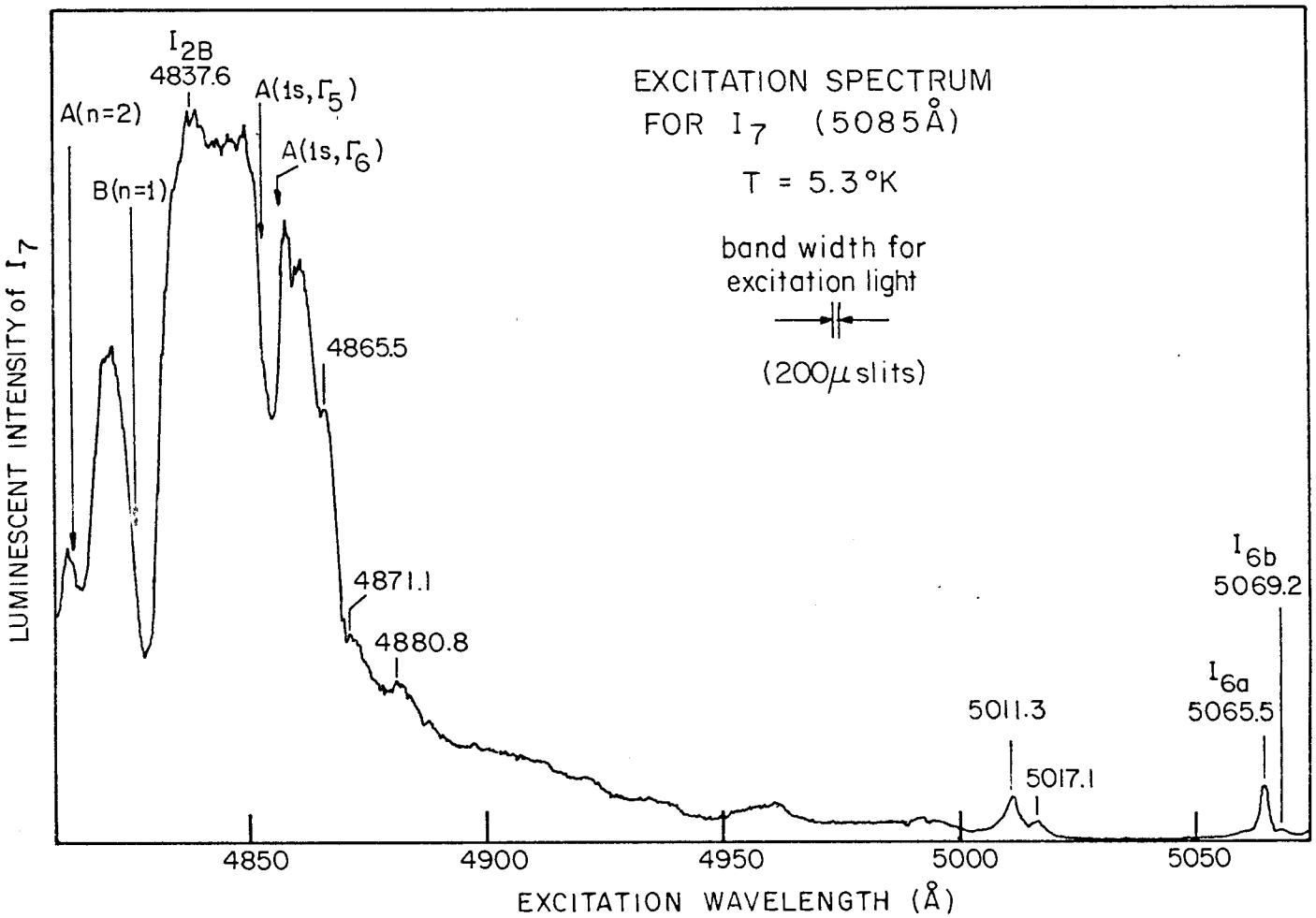

Fig. 15 Excitation spectrum for the I_7 luminescent transition. The appearance of this spectrum was essentially independent of the intensity of the long wavelength lines relative to the $I_{2o} \rightarrow 1s$ transition.

at 5011.3Å, 5017.1Å, and at the I_{6a} and I_{6b} transitions in Fig. 15. Further evidence of this coupling is given by the fact that in samples where I_7 is very weak, the I_6 lines at longer wavelengths are enhanced.

7.2 Temperature Dependence of Emission Intensity

The emission intensity of the I_6 and I_7 lines was measured for temperatures between 5°K and 115°K. The qualitative effects of increasing temperature are illustrated in Fig. 16. I_{6b}, I^1_{6b}, I^2_{6b} and I^3_{6b} behave in a similar manner, decreasing considerably in intensity as the temperature is raised. I_{6a} and I^2_{6a} remain strong, with I_{6a} showing a slight increase in intensity. This is consistent with the assumption that I_{6a} and I^2_{6a} are transitions from an excited state of the I_6 complex since, as temperature is raised, decay will tend to occur from the excited state due to thermal pumping from the ground state. The intensity of I^2_{6a} decreases slightly since this transition terminates on an excited final state, and will be somewhat thermalized as temperature is raised. Plotting $\ell n(I_{6a}/I_{6b})$ vs. $1/T$ yields an activation energy $\Delta E \sim 0.5$mev (see section 6.3).

The I_7 transition is completely quenched by about 20°K. This rapid drop in intensity may be due to some interaction with the I_6 complex. For example, if the two centers are in

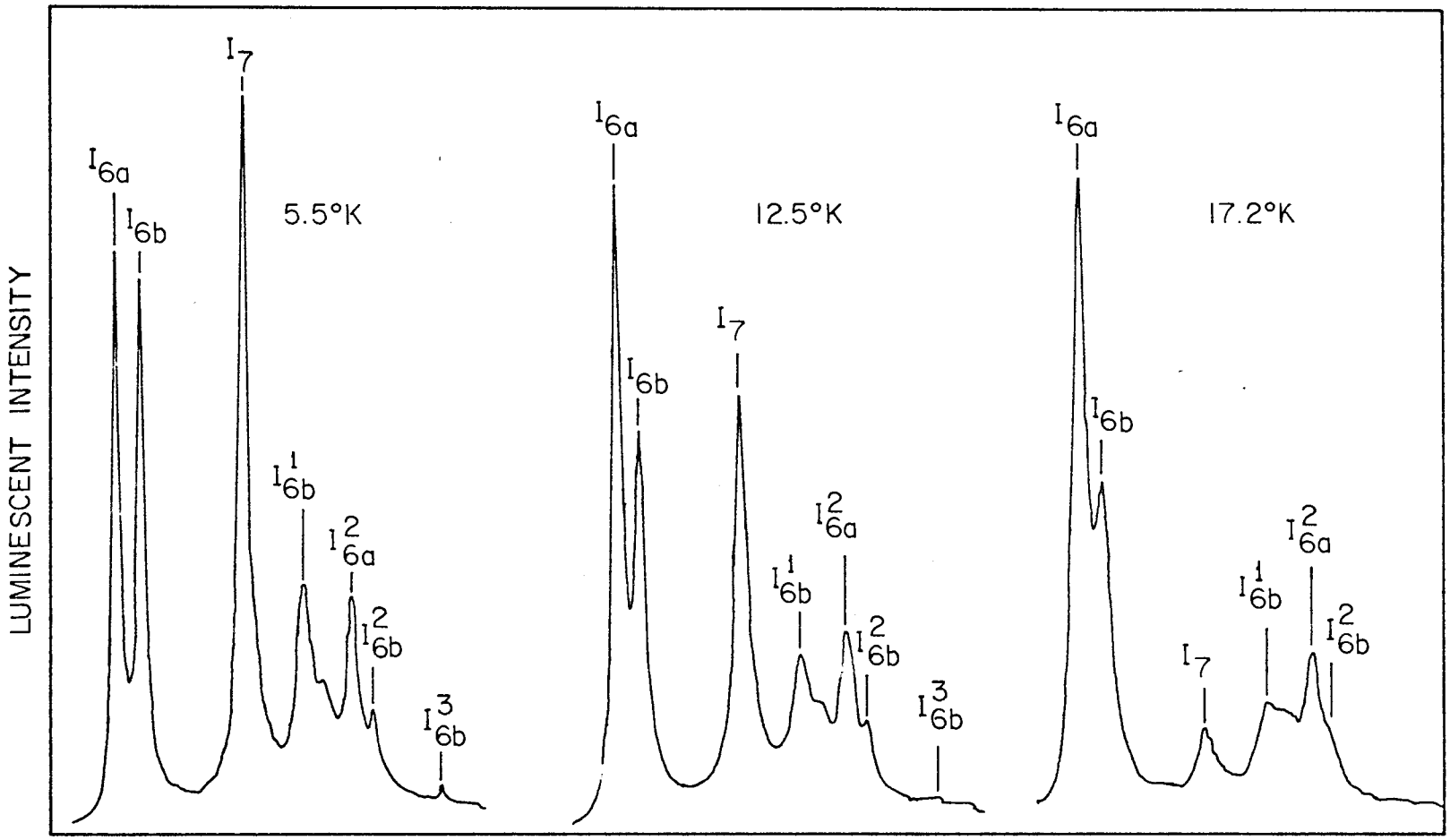

Fig. 16 Qualitative effects of temperature variation on the long wavelength lines.

close proximity, it may be energetically favorable for I_6 to capture some constituent part of I_7 as the latter is thermally excited. This may be why no apparent excited states of I_7 are observed.

Due to the close proximity of the I_6 and I_7 lines, it was possible to do quantitative thermal quenching only for I_{6a}. This line becomes very dominant beyond about 20°K and may easily be observed at temperatures as high as 115°K. A plot of $\ell n(I_{6a})$ vs. 1/T appears in Fig. 17. From the high temperature thermal quenching region (see eqn. 6.3.4) an accurate estimate of the thermal activation energy $E_a(I_{6a})$ can be made. We find:

$$E_a(I_{6a}) = 43.2 \pm 0.2\text{mev.}$$

The uncertainty quoted is the standard error from a least-squares fit calculation. The value of $E_a(I_{6a})$ agrees well with the value of 43 ± 3mev for the low energy cut-off of band A in Fig. 11. This is reasonable since the I_6 luminescence will be quenched when the least bound part of the exciton may be removed. This is in contrast to weakly bound excitons such as I_2 where the exciton may dissociate from the impurity center intact. Thus the observed thermal activation energy for the $I_{2o} \rightarrow$ ls transition should be equal to the binding energy of the A exciton to the Cl donor.

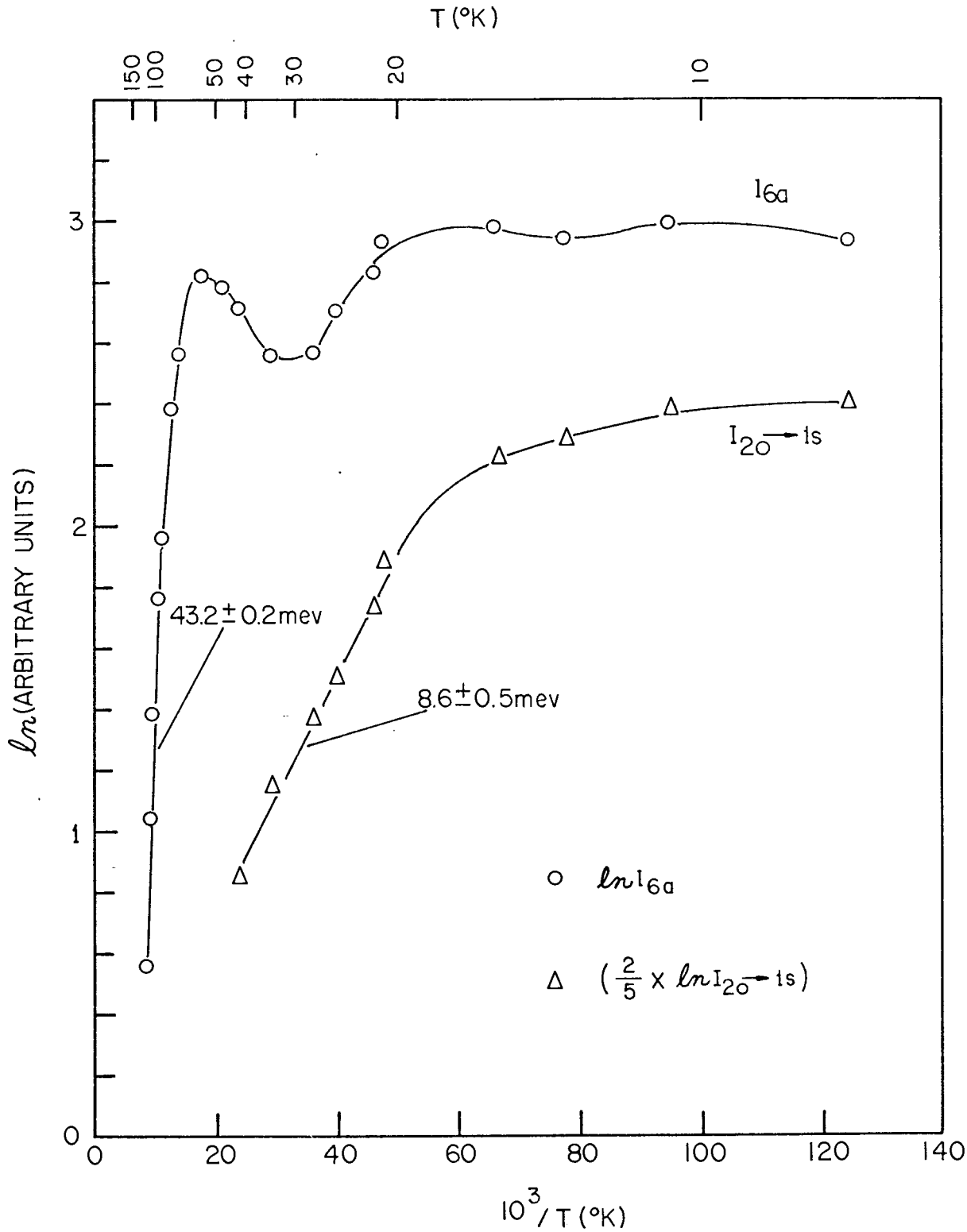

Fig. 17 Temperature dependence of the I_{6a} and $I_{2o} \rightarrow 1s$ transitions illustrating thermal quenching at higher temperatures. The vertical ℓn scale for $I_{2o} \rightarrow 1s$ has been multiplied by a factor of 2/5 to allow it to conveniently plotted with I_{6a}.

We find from our measurements:

$$E_a(I_{2o} \rightarrow 1s) = 8.6 \pm 0.5\text{mev}$$

in agreement with the value of 8.5mev determined by the energy difference between the $A(1s,\Gamma_5)$ and $I_{2o} \rightarrow 1s$ transitions for our samples.

The small resonances at low temperatures in Fig. 17 may be due to thermal activation of the I_{6b} and I_7 lines. The resonance at higher temperatures coincides with the temperature region of rapid quenching of the $I_{2o} \rightarrow 1s$ luminescence. Thus this resonance may be due to an enhanced probability of free exciton capture, due to thermal ionization of excitons from the I_2 complex.

7.3 Dependence on Excitation Intensity

By means of neutral density filters the intensity I_i of band-gap light, incident on a crystal, was varied to measure the effect on the long wavelength lines. If I_o is the intensity of light incident on a neutral density filter of index n, then the following relationship holds:

$$n = \log (I_o/I_i) \Rightarrow I_i = I_o(10^{-n}) \qquad 7.3.1$$

If we assume that the intensity I_{LUM} of luminescent light emitted by the crystal has a simple power dependence

$$I_{LUM} = BI_i^x \qquad B = \text{const.} \qquad 7.3.2$$

then it is easy to see that

$$\log(I_{LUM}) = \text{const} - nx \qquad 7.3.3$$

from eqn. 7.3.1. $\text{Log}(I_{LUM})$ is plotted against n in Fig. 18 for the five most intense long wavelength lines. The qualitative effects of variations in intensity may be seen in Fig. 19.

All lines in Fig. 18 exhibit superlinear intensity dependence at lower excitation intensities (higher values of n). This behavior is common for bound exciton emission (see, for example, Maeda 1965). At low excitation intensities I_{6b} is considerably stronger than I_{6a}. This is reasonable since I_{6a} results from an excited state and rapid relaxation to the ground state may take place. This is evidenced by the strong resonance at I_{6a} in Fig. 13.

At higher excitation intensities, I_{6b} and I^1_{6b} both saturate and exhibit sublinear intensity dependences. This effect will occur due to a decrease in the probability of nonradiative transitions from I_{6a} to I_{6b}, as a result of filling the ground state. This view is supported by the fact that I_{6a} and I^2_{6a} do not show saturation effects in this region.

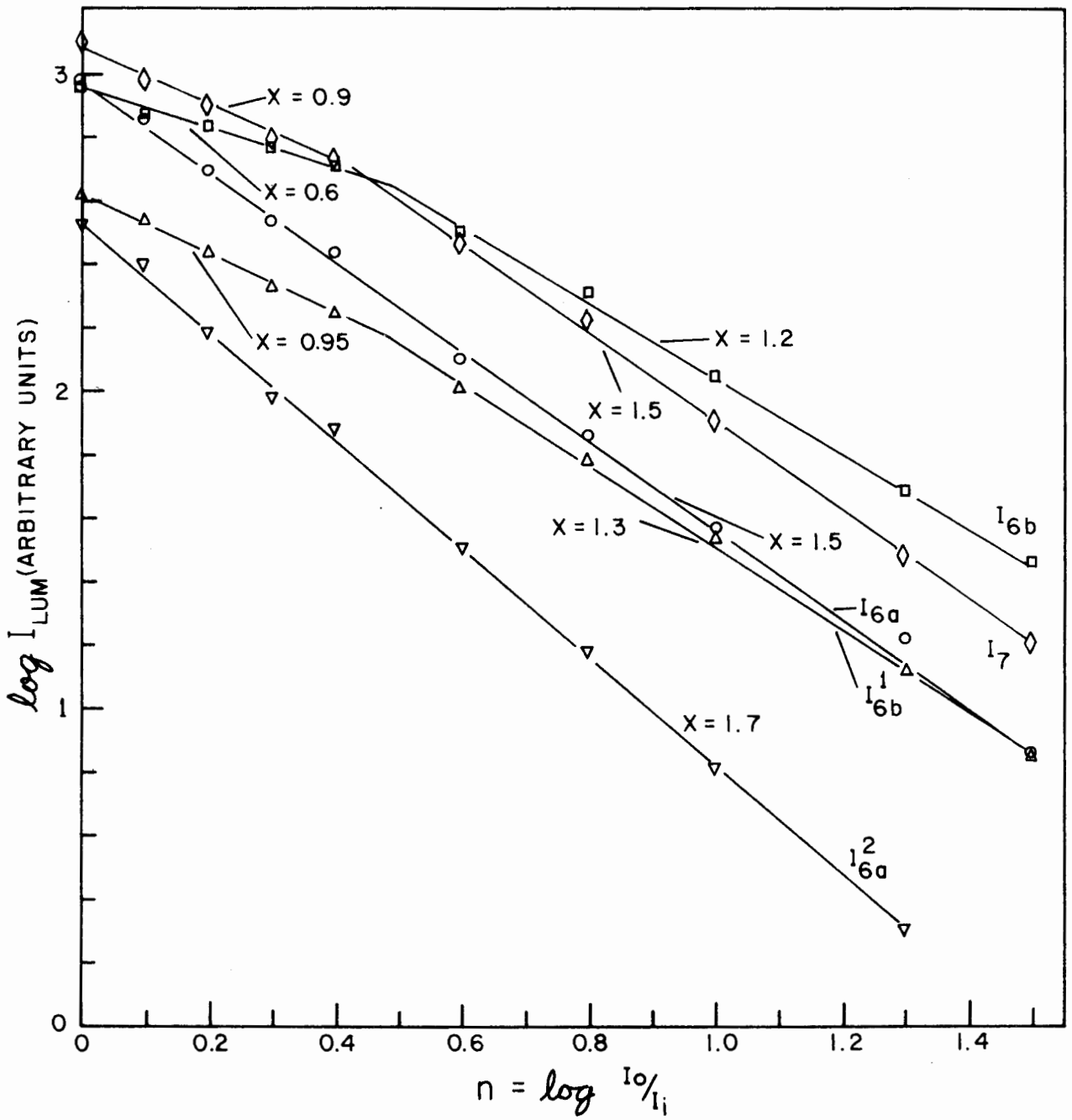

Fig. 18 Intensity dependence of the stronger long wavelength transitions. Saturation effects are shown by I_7, I_{6a} and I^1_{6a}, as indicated by a reduction in slope for these lines at higher excitation intensities (smaller values of n).

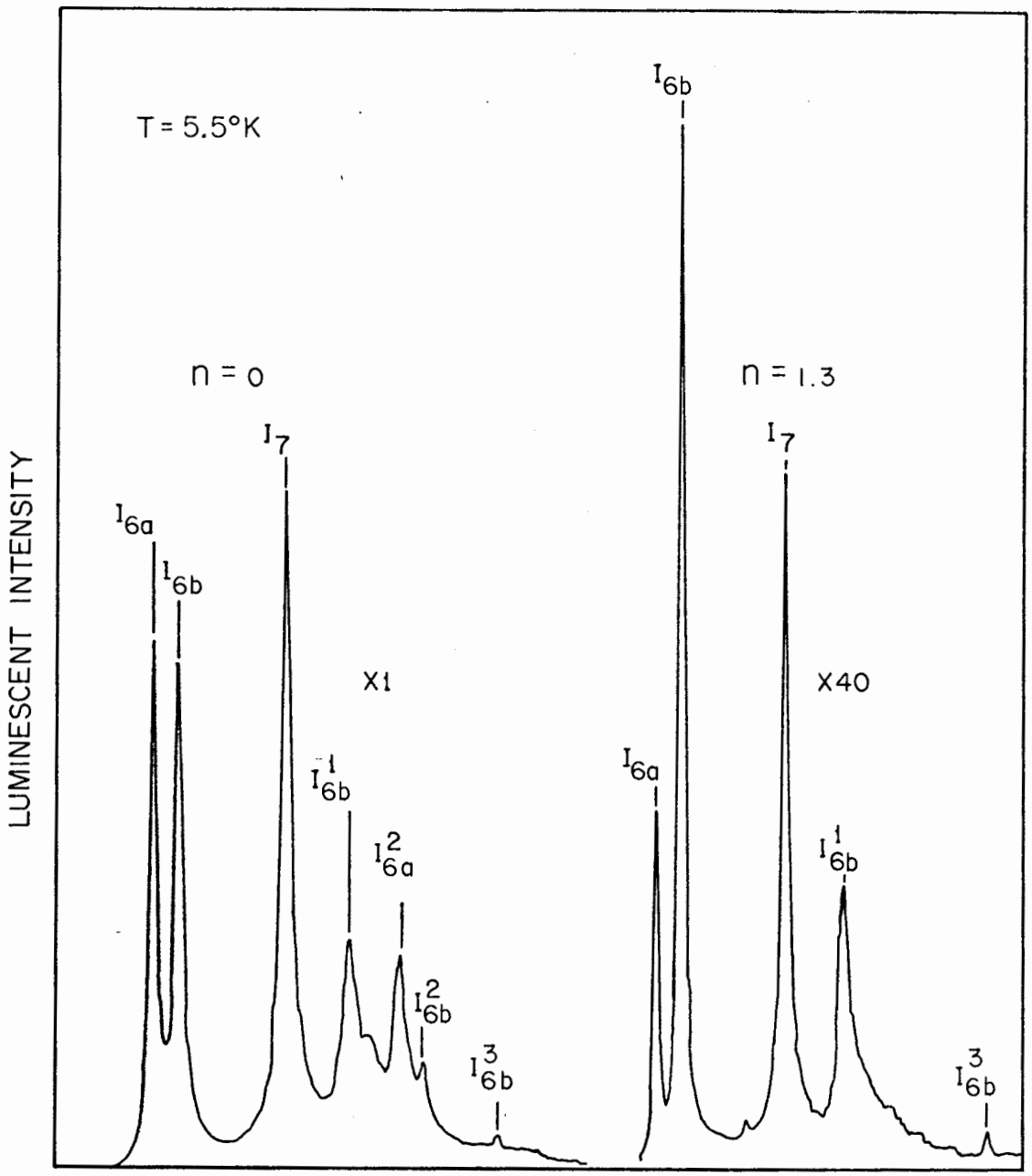

Fig. 19 Qualitative effects of variation of excitation intensity on the long wavelength lines. n is defined in equation 7.3.1.

7.4 Infrared Irradiation

Near infrared radiation of about 1.5 to 0.4ev was provided by using a 75 Watt Xeon arc lamp in series with a Corning 7-57 filter. The long wavelength lines were excited with a minimum of band-gap light, and emission spectra were recorded both with and without I.R. irradiation. The results are presented in Fig. 20.

Thomas and Hopfield (1962) performed a similar experiment on an n-type CdS crystal in order to investigate the behavior of the I_2 and I_3 bound exciton complexes. They postulated that I.R. radiation in the region 1.5 to 0.4ev ionizes neutral acceptors to produce free holes, which may then react with electrons on neutral donors to produce ionized donors. Thus I.R. radiation was found to favor ionized centers, causing an increase in the intensity of I_3 and a corresponding decrease in I_2 emission.

In our experiment, however, the $I_{2o} \rightarrow 1s$ transition was essentially unaffected by infrared irradiation. This indicates that the liberated holes are being recaptured by centers other than neutral donors. The corresponding large increase in intensity for the long wavelength lines under I.R. irradiation, illustrated in Fig. 20, indicates that the I_6 and I_7 centers are capturing the liberated holes. This also indicates that electrons must have previously been

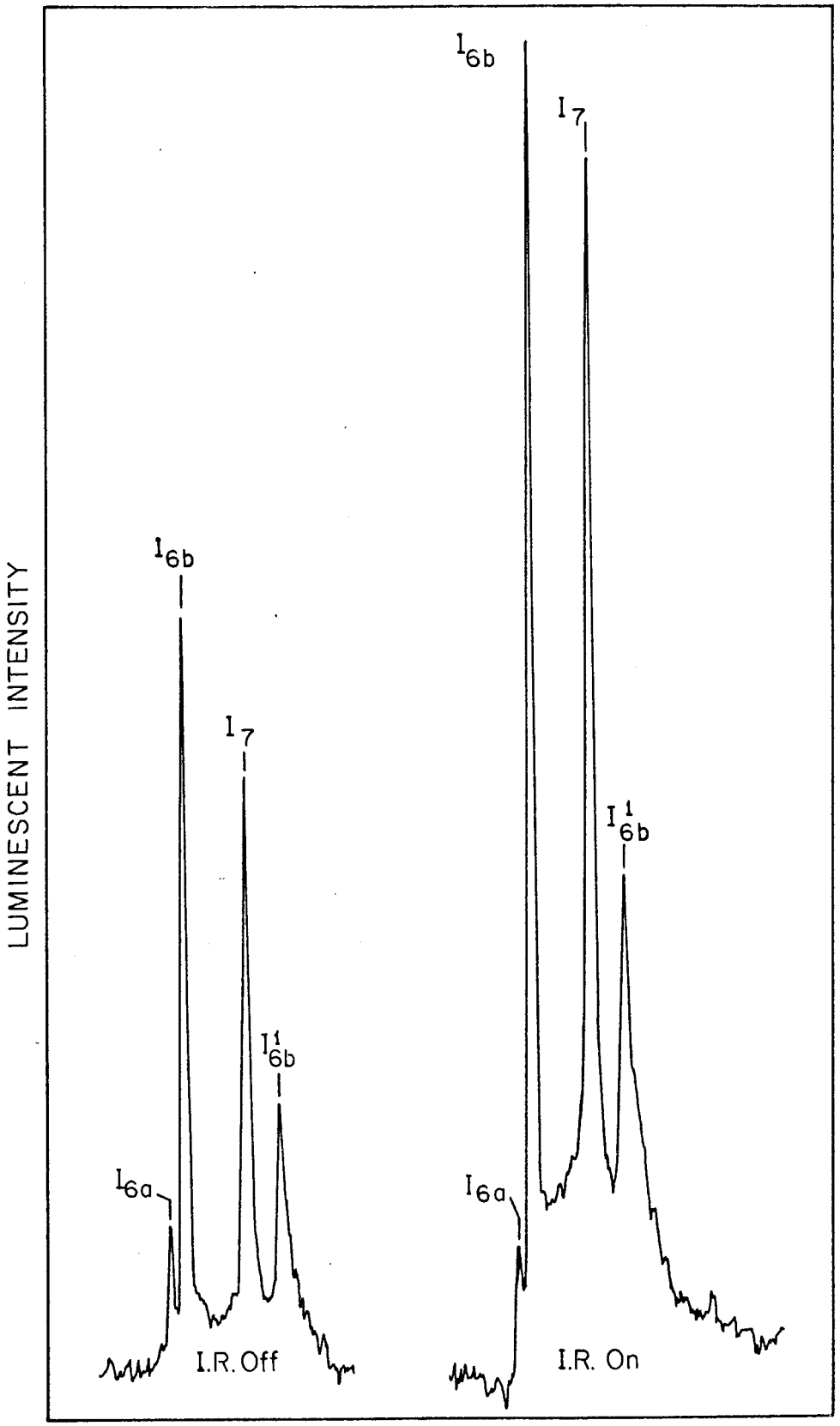

Fig. 20 The qualitative effect of infrared irradiation on the long wavelength lines. T ≈ 5°K.

captured by the I_6 complex, in agreement with the assumption in section 7.1.2 that the I_6 electron traps will be filled from Cl donors.

7.5 Energy Level Diagram for Decay of the I_6 Complex

On the basis of our experimental results an energy level diagram has been constructed in Fig. 21. The superscripts on the transition labels refer to different terminal states. The identification of I_{6b}^3 and I_{6b}^4 is only tentative, as indicated by broken lines. The physical meaning of the terminal states for the I_6 transitions cannot be inferred from Fig. 21. In analogy with the two-electron transitions in Fig. 4, it is believed that they represent states of the impurity center giving rise to the I_6 complex.

With regard to the states of the I_6 complex, it is interesting to note that a splitting of 1.6mev is observed for the ground state of an exciton bound to an Oxygen isoelectronic trap in ZnTe, due to j-j coupling of the electron and hole (Merz 1968). It would be worthwhile to investigate the Zeeman splitting of I_{6a} and I_{6b} to see if an analogous effect is occurring in CdS. Unfortunately we were not equipped to perform experiments with magnetic fields.

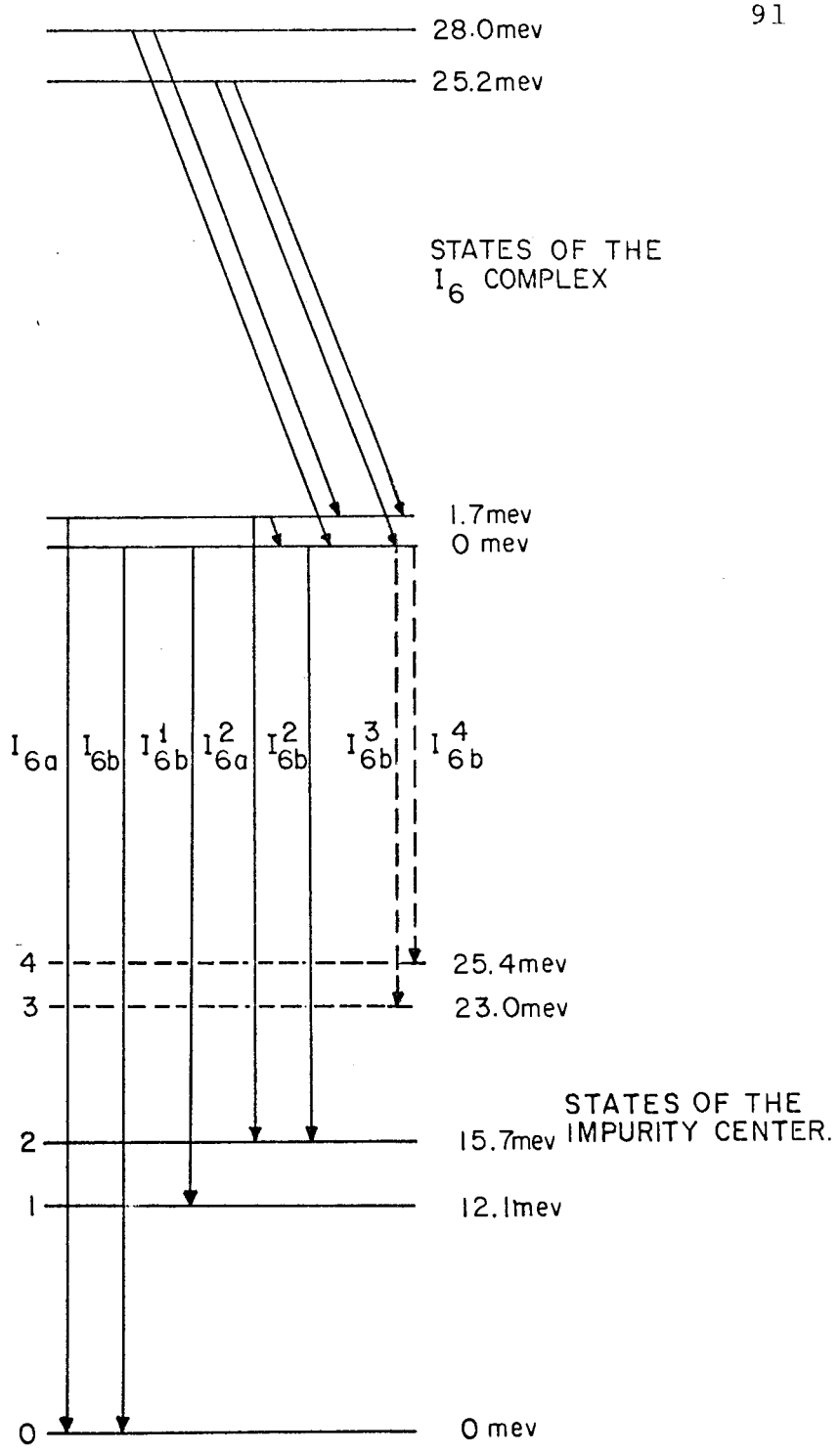

Fig. 21 The most probable decay configuration for the I_6 complex, based on experimental data. The transitions marked with broken lines are more tentative than those marked with solid lines.

7.6 Summary and Conclusions

We have reported the existence of a series of sharp long wavelength lines in CdS, including two transitions originally observed by Reynolds and Litton (1963). On the basis of experimental observations we have concluded that the I_6 and I_7 lines arise from two chemically distinct impurities. From the interpretation of excitation spectra we have suggested that the center producing the I_6 long wavelength emission is capable of binding one particle, probably a hole, by about 43mev and the oppositely charged particle by about 104mev. This is supported by thermal quenching experiments which yield a thermal activation energy of 43.2 ± 0.2mev for the I_{6a} line.

A diagram illustrating the most probable decay configuration for the I_6 complex has been constructed in Fig. 21. The final states of the illustrated transitions have been identified as low lying states of the impurity center producing the I_6 luminescence. Since little is known about the electronic structure of deep impurities, the theoretical interpretation of these levels is not clear.

If the center is an isoelectronic trap the final states could be imagined as valence band states which have been distorted by strong local fields, produced by misfit of the isoelectronic center in the host lattice. The relative

separation of levels 0, 1, and 2 in Fig. 21 is somewhat suggestive of the valence band splitting illustrated in Fig. 1. For transitions between these band states to occur, however, requires that they be partially unoccupied. This appears to be highly unlikely even under conditions of non-thermal equilibrium produced by the presence of excitation light.

If the impurity center giving rise to I_6 is a deep donor or acceptor, the final states might be one particle energy levels observed due to excitation of the residual electron or hole. This would be somewhat analogous to the two-electron transitions discussed in sections 4 and 5, but in this case the final states would not be hydrogenic. In any event, further work is indicated in this area. Future research might involve such areas as investigation of the magnetic properties of the long wavelength lines, infrared absorption measurements, or investigation of the effects of sample treatment. Improved knowledge of the structure of the I_6 complex will prove useful in understanding the behavior of deep centers in CdS.

REFERENCES

Abramowitz, M. and Stegun, I.A., 1968. Handbook of Mathematical Functions (Dover, New York), p.537

Berlincourt, D., Jaffe, H. and Shiozawa, L.R., 1963. Phys. Rev. 129, 1009

Bohm, D., 1951. Quantum Theory (Prentice-Hall, New York), p.508

Conradi, J., 1968. Ph.D. Thesis, Simon Fraser University

Czyzak, S.J., Baker, W.M., Crane, R.C. and Howe, J.B.,1957. J. Op. Soc. Am. 47, 240

Dexter, D.L., 1953. J. Chem. Phys. 21, 836

Dexter, D.L. and Knox, R.S., 1965. Excitons (Wiley, New York)

Dow, J.D., 1968. Phys. Rev. 174, 962

Dumke, W.P., 1963. Phys. Rev. 132, 1998

Faulkner, R.A. and Dean, P.J., 1970. J. of Lum. 1,2, 552

Henry, C.H., Faulkner, R.A. and Nassau, K., 1969. Phys. Rev. 183, 798

Henry, C.H. and Nassau, K., 1970a. Phys. Rev. B1, 1628

Henry, C.H. and Nassau, K., 1970b. Phys. Rev. B2, 997

Henry, C.H., Nassau, K. and Shiever, J.W., 1970. Phys. Rev. Lett. 24, 820

Hopfield, J.J., 1959. J. Phys. Chem. Solids 10, 110

Hopfield, J.J., 1960. J. Phys. Chem. Solids 15, 97

Hopfield, J.J. and Thomas, D.G., 1960. J. Phys. Chem. Solids 12, 276

Hopfield, J.J. and Thomas, D.G., 1961. Phys. Rev. 122, 35

Hopfield, J.J., 1964. Proceedings of the 7th International Conference on the Physics of Semiconductors (Paris), ed. M. Hulin (Dunod, Paris), p.725

Hopfield, J.J., Thomas, D.G. and Lynch, R.T., 1966. Phys. Rev. Lett. 17, 312

Johnson, E.J., 1968. Semiconductors and Semimetals vol. 3, ed. R.K. Willardson and A.C. Beer (Academic Press, New York), p.201

Knox, R.S., 1963. Theory of Excitons (Academic Press, New York)

Kohn, W., 1957. Solid State Phys. 5, 258

Kukimoto, H., Shionoya, S. and Kamejima, T., 1971. J. Phys. Soc. Japan 30, 1662

Maeda, K., 1965. J. Phys. Chem. Solids 26, 1419

Malm, H., 1971. Ph.D. Thesis, Simon Fraser University

Malm, H. and Haering, R.R., 1971a. Can. J. Phys. 49, 2432

Malm, H. and Haering, R.R., 1971b. Can. J. Phys. 49, 2970

Merz, J.L., 1968. Phys. Rev. 176, 961

Messiah, A., 1966. Quantum Mechanics vol. 2 (North-Holland, Amsterdam), p.742

Morgan, T.N., Pilkuhn, M. and Rupprecht, H., 1965. Phys. Rev. 138, A1551

Nassau, K., Henry, C.H. and Shiever, J.W., 1970. Proceedings of the Tenth International Conference on the Physics of Semiconductors, ed. S.P. Keller, J.C. Hansel and F. Stern (U.S. Atomic Energy Commission), p.629

Neuberger, M., 1969. II-VI Semiconducting Compounds Data Tables (Clearinghouse for Federal Scientific and Technical Information, Springfield, Va., U.S.A.)

Peierls, R., 1932. Ann. Phys. 13, 905

Reynolds, D.C. and Litton, C.W., 1963. Phys. Rev. 132, 1023

Reynolds, D.C. and Collins, T.C., 1969. Phys. Rev. 188, 1267

Schiff, L.I., 1968. Quantum Mechanics 3rd edition (McGraw-Hill), p.292

Shionoya, S., 1970. J. of Lum. 1,2, 17

Tell, B., Damen, T.C. and Porto, S.P.S., 1966. Phys. Rev. 144, 771

Tell, B., 1970. J. Appl. Phys. 41, 3789

Thomas, D.G. and Hopfield, J.J., 1959. Phys. Rev. 116, 573

Thomas, D.G. and Hopfield, J.J., 1962. Phys. Rev. 128, 2135

Wannier, G.H., 1937. Phys. Rev. 52, 191

Yakobson, M.A., 1966. Optics and Spectrosc. 20, 40